Inferring Hydrogeologic Processes with Distributed Temperature Sensing in Indian River Bay, Delaware

Robert B. Carver

Department of Earth and Planetary Sciences

McGill University

Montreal, Quebec, Canada

May 2012

A thesis submitted to McGill University in partial fulfillment of the requirements of the degree of Master of Science

TABLE OF CONTENTS

LIST OF TABLES

LIST OF FIGURES

ABSTRACT

The interaction between coastal aquifers and estuaries governs many important ecological and water quality processes. The purpose of this research is to use distributed temperature sensing (DTS) in the Indian River Bay estuary, Delaware, to detect differences in variance and mean of temperature at the sediment-water interface. DTS uses the scatter of laser light in a fibre optic cable as a means to repeatedly measure temperature to 0.1˚C at 1m intervals along the length of the cable. Low variances in temperature are interpreted as being the result of the moderating thermal influence of groundwater discharge. From September 16 to 19 2011, two kilometres of DTS cable were deployed in the near shore environment of Holts Landing State Park. Variance increases with distance from shore as the power function $s^2=-33.63(d^{(-1.012)}) + 2.685$ ($r^2=0.78$). Narrow zones with significantly lower temperature variances (Kruskal-Wallis with Tukey's HSD, $p<0.05$) and means (Friedman with Tukey's HSD, $p<0.05$) than adjoining zones exist within the near shore area. Zones of high variance at the western and eastern edges of the study site are associated with ancient shallow peat-filled valleys capped with fine sediments. A broad zone of low variance next to the western valley is interpreted to imply that over-pressured fresh groundwater is discharging at the paleo-valley margins, creating a pattern of submarine groundwater discharge which differs from existing models. An attempt to use diurnal temperature signal amplitudes at various sediment depths to calculate vertical porewater flux were unsuccessful, likely due to rapidly-rising temperatures, interference between tidal and diurnal signals, and a short measurement period. DTS appears to hold promise in detecting temperature patterns simultaneously across different scales, and can be used to rapidly fill in gaps of knowledge in hydrogeologic systems.

RÉSUMÉ

Les interactions entre les aquifères côtiers et les estuaires régissent beaucoup de processus écologiques importants qui ont des implications sur la qualité de l'eau souterraine et marine. La compréhension de la nature et de l'ampleur de ces interactions est devenu un foyer de recherches, facilité par des avances récentes dans notre capacité de détecter la décharge submersible d'eaux souterraines. Cette étude emploie la détection distribuée de température (DDT) dans l'estuaire de la baie Indian River, sur la côte du Delaware, afin de détecter des différences dans la variance et la moyenne de la température des eaux à l'interface entre la baie et le sédiment dans la zone près du rivage du parc Holts Landing. Des variances basses sont interprétées comme étant le résultat de l'influence de modération des eaux souterraines, compatible avec les autres études, et le fait que les zones peu profondes près du rivage, qui devraient éprouver plus de variation de la température que des zones plus profondes, sont au contraire plus stables. La variance augmente avec la distance du rivage à mesure que la fonction s^2=-33.63 ($d^{(-1.012)}$) +2.685 (r^2=0.78). Près du rivage, il y a des endroits étroits avec des variances (Kruskal-Wallis avec Tukey's HSD, $p<0.05$) et moyens (Friedman avec Tukey's HSD, $p<0.05$) sensiblement plus basse que leurs zones proximales. Des zones de la variance élevée aux bords a l'ouest et l'est de l'emplacement d'étude sont associées aux anciennes vallées peu profondes remplies de la tourbe et maintenant couvertes avec les sédiments fins. Une large bande de bas désaccord à côté de la vallée occidentale implique que les eaux souterraines fraîches sosu pression élevée coulent aux marges de la vallée, créant un modèle du SGD qui n'équipe pas des modèles précédents. Une tentative d'employer des amplitudes de signal de la température à de diverses profondeurs de sédiment pour calculer le flux vertical d'eau interstitielle a échoué, probablement en raison des temperatures croissantes, interférence entre les signaux de la marée et diurne, et une période d'échantillon courte. DDT semble tenir la promesse en détectant des tendences de la température à travers différentes gammes simultanément, et peut être employé pour trouver les pieces manquantes de la connaissance des systèmes hydrogéologiques.

ACKNOWLEDGEMENTS

There are many who must be thanked for their kind and generous support in helping me put together this thesis. First, Dr. Jeffrey McKenzie, for his trust in me. His patience was unwavering as I tested the water, so to speak, on several projects, and his enthusiasm for my pet pursuits sometimes seemed to exceed mine. Dr. Michel Baraer was also a patient mentor to me, never annoyed at my treating him as a sounding board for my many half-baked ideas, and answering my too-many questions about MATLAB, signal processing, and scientific rigour. Danny Chavez challenged my thinking, tested my fundamental hydrological knowledge, and drank a lot of salt water helping me collect data and for that I am grateful. Laura Maharaj, with her cheery disposition and love of people, set the tone at the beginning of my work, and her presence still pervades our department.

I would also like to thank our wonderful hosts at UDel who helped collect and organize the data at Holts Landing: Chris Russoniello, Cristina Fernandez and Holly Michael. Scott Andres also found time to cheerfully answer my questions about the area around our study site, despite our never having met.

The Department of Earth and Planetary Sciences provides its students with a warm, supportive, familial environment, and here I learned that school is about both life and learning. Thanks to all the staff and faculty who make that happen.

Finally, I thank my family. My parents and brother have always been there for me when I needed them. Lise, my wife, has been unwavering in making sure that I can balance this project with life at home. My daughter Emma is always there to give me hugs when it looks like I need them and Théo makes sure I get up every morning early for work! They are the joys of my life, and they get me through the days.

Introduction

Groundwater and surface water interactions in coastal environments are the focus of a growing number of studies. These interactions have implications for natural and engineered processes and systems, including benthic ecosystems (Peterson et al. 2012), coastal aquifer management (Duarte et al. 2010), nitrogen fixation (Rao and Charette 2012) and contaminant transport (Slater et al. 2010). Eutrophication of estuary environments, and the role that groundwater plays in nutrient transport to these systems, is of particular interest given their economic, ecological and social importance (Johannes 1980; Kennish 2000). While it has become increasingly clear that submarine groundwater discharge (SGD) into estuaries has been overlooked as an important nutrient source, researchers have struggled to quantify the extent of SGD, the processes that control it, and the implications for the systems where it occurs (Johannes 1980; Michael et al. 2003; Michael et al. 2005; Michael et al. 2011). These include coastal groundwater systems, estuaries, and the benthic environments at the interface of these systems (Simmons 1992; Burnett et al. 2006).

A major challenge in studying SGD is measuring the flux of groundwater at the sediment/water interface. Direct methods such as seepage meters (Lee, 1977; Lee and Cherry, 1978) are commonly used, but these often fail to detect or account for important heterogeneities at local scales. Michael et al. (2003) acknowledge this, and attempt to answer the question 'How many meters are necessary?' to capture the desired level of detail. Piezometers provide information on hydraulic gradients but installation can be labour intensive, hydraulic conductivity values are poorly constrained, and the point data they provide also suffer from problems of scalability (Hatch et al. 2006). Studies using natural or artificial tracers such as dye (Cable and Martin 2008), major ions (Mondal et. al 2010), radon (Burnett 2006; Kim et al. 2003), radium (Michael et al. 2011; Rapaglia et al. 2012), helium and hydrogen isotopes (McCoy et al. 2007) or any combination of these, provide indirect measurements of flux but can be time-consuming, expensive, and difficult to execute

(Rapaglia et al. 2012). Hatch et al. (2006) present a summary of the traditional flux measurement methods and their associated advantages and disadvantages.

Temperature can also be used as a tracer. Stallman (1965) presented an equation for calculating the vertical flux of porewater from subsurface temperatures, although the method was not well-suited for natural conditions. Lapham (1989) developed a numerical model to solve the partial differential equation which governs the flow of heat and water in sediment, and used it to back-calculate hydraulic conductivity. Taniguchi and Sharma (1993) conducted early field experiments and successfully calculated soil water recharge. Stonestrom and Constantz (2003) describe and summarize heat-based methods to measure groundwater fluxes near streams, while Anderson et al. (2005) provide a comprehensive review of the history of the use of heat in groundwater tracing.

Recent advances in measurement technology allow us to measure temperature not only at discrete points, but continuously along a fibre-optic cable for distances up to several kilometres (Selker et al. 2006). This distributed temperature sensing (DTS) provides a means to easily detect differences in temperature at metre- and minute- scales, thereby overcoming some of the limitations of previous methods. However, DTS as a hydrological research tool is still in its infancy and much work needs to be done to define best practices and explore the potential and limitations of this technique.

SUBMARINE GROUNDWATER DISCHARGE

High nutrient concentrations in estuary settings have long been associated with eutrophication (Valiela, 1992; Davis and Kratzer, 1996; Morand and Briand, 1996), though until recently the role of SGD in nutrient transport to coastal waters had been largely neglected (Bokuniewicz, 1980; Johannes, 1980; Bokuniewicz, 1992). Recent work has shown that SGD makes up a surprisingly large fraction of the total water and nutrient contribution to coastal areas. Moore (2010) describes SGD as an important, yet underestimated, vector for nutrients, carbon and metals, and shows that SGD along parts of the southeast coast of the USA likely exceeds river flows by a factor of three. Szymczycha et al. (2012) discovered that SGD is a significant contributor of phosphorous to the Baltic Sea, and Null et al. (2012) found that groundwater contributes high levels of both phosphorous and nitrogen to San Francisco Bay. Weinstein et al. (2011) pointed out that much SGD is actually nutrient-poor recirculated seawater, but still found that it was a major contributor of terrestrially-derived nitrogen and silica to Dor Bay in the eastern Mediterranean. Nutrient-rich SGD has also been implicated in elevated primary production along the Yucatan Peninsula (Troccoli-Ghinaglia et al. 2010), variable oyster production in Japan (Hosono et al. 2012), and algal blooms off the coast of Florida (Smitha and Swarenskib, 2012).

The manner in which SGD enters coastal systems is not well understood, although models of these interactions have evolved as SGD has become more of a research focus (Burnett et al. 2006). Though it is not germane to the current study, one model deals with SGD that occurs in fractured, karstic or volcanic terrains, where water flows underground via open conduits to the sea, emerging as a highly localized fresh plume some distance from the shore (Fleury et al. 2007; Dimova et al. 2012). For more typical settings dominated by Darcian flow, the foundation of modern models is the stable Dupuit-Ghyben-Herzberg fresh-water lens, where the only interaction between fresh and salt water is deemed to occur at the tip of the lens where it meets the sea at the shore. Hubbert (1940) pointed out that this arrangement is unsustainable if there is no movement of saline groundwater, thus introducing the concept of a wider interface that does not necessarily reside at the shoreline, but extends beneath the shore sediments and under the surface water body. Bear et al. (1999) reviewed SGD measurement methods and models which incorporate controls on flow such as tides, withdrawals, stratigraphy, topography and density differences, and describe a thicker transition zone where fresh and saline waters mix somewhat. Michael et al. (2005) found that seasonal changes in the water table is a driving force for salt water to move into and out of the groundwater system on an annual basis, with seaward fluxes lagging upland recharge by up to several months. Figure 1 summarizes the water fluxes and their forcings at shore zones.

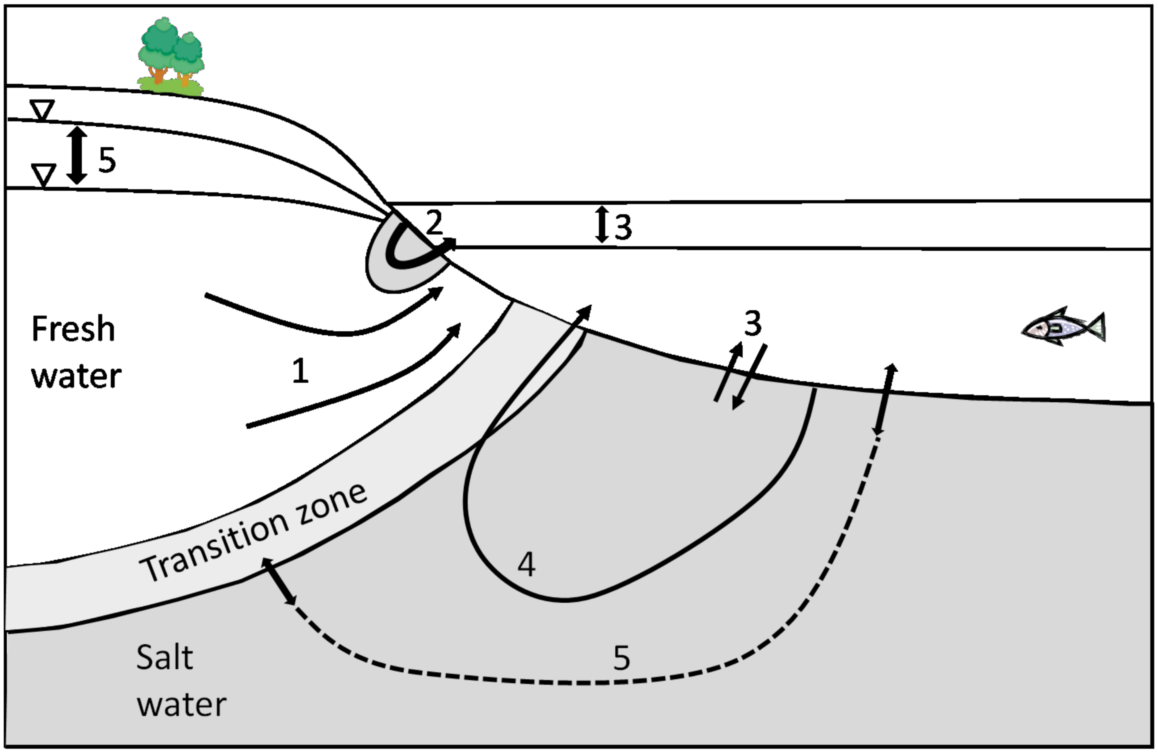

Figure 1 Saline and fresh water fluxes in tidal environments, comprising 1) seaward flow of fresh water due to hydraulic head differences, 2) salt water recirculation at the shore zone due to wave and tidal action, 3) porewater flux due to tides and waves, 4) density-driven flow and 5) large fluxes of water and salt due to movement of the transition zone on lunar, seasonal or other timescales. Adapted from Michael et al. (2011).

The interface where salty ocean water meets and mixes with fresh groundwater has been described as a subterranean estuary (Moore, 1999). The processes that occur within this estuary are important controls on the quality and volume of groundwater that enters the sea. For example, residence (or flushing) time will affect the opportunities for biogeochemical interactions between groundwater and estuary sediments, which may act as a nutrient source or sink (Statham, 2012). Charette and Sholkovitz (2002) showed that sediments rich in iron oxides create an 'iron curtain' that is potentially capable of sequestering large amounts of contaminants and nutrients. Charette et al. (2005) found that in a subterranean estuary at Waquiot Bay, MA, uranium and barium are adsorbed by oxides of iron and manganese, respectively. Whether solutes are sequestered or released in these settings is dependent on dissolved oxygen levels and the oxidation state of estuary sediments. Under oxic conditions, phosphorous is sequestered in this layer of iron oxides (Charette and Sholkovitz, 2002; Burdige, 2006), and nitrate remains in solution (Denver et al. 2004; Rao and Charette, 2012). Conversely, anoxia can lead to rapid phosphorous release and denitrification (Denver et al. 2004; Rao and Charette, 2012; Statham, 2012). Accounting for this variability requires an understanding of the heterogeneity of the subterranean estuary and its processes in both time (Michael et al. 2005) and space (Andres, 1992).

The idea that scale is an important consideration in SGD investigations was highlighted by Bratton (2010), who describes three spatial scales comprising the nearshore scale (within 10 m of shore) consistent with the Ghyben-Herzberg and Hubbert models, the embayment scale (10 to 104 m from shore) where outcrops of confined aquifers meet the sea bottom to produce submarine springs, and the shelf scale, which includes the width and breadth of all continental shelf aquifers. He argues that scientific findings should be integrated across scales. Similarly, Burnett et al. (2006) recommend that SGD investigations include measurement strategies that can detect patterns of SGD decreasing as a function of distance from shore and changing as a function of diurnal and lunar tidal cycles.

DISTRIBUTED TEMPERATURE SENSING

The measurement of temperature using glass core fibre-optic technology dates back to at least the mid-1980s (Dakin et al. 1985; Hartog et al, 1985). The technique relies on the scattering that occurs when a pulse of laser light in a fibre-optic line interacts with the opaque cladding surrounding the clear core (Figure 2c) and is scattered back to a photon detector. Distance to the point of scatter can be calculated by measuring the two-way travel time. Some of the scattered light is lower in frequency than the incident light (Stokes scatter), while an equal portion is scattered at a higher frequency (Anti-Stokes). There are two frequency peaks (Brillouin and Raman) on each side of the incident frequency (Figure b).

While neither peak of Stokes scattering is influenced by temperature, the amplitude of the Anti-Stokes Raman peak is temperature-dependent. Therefore, the ratio between Stokes and Anti-Stokes Raman amplitudes can, with calibration, be converted to temperature. The Brillouin peak is temperature- and strain-sensitive, making it unsuitable for DTS work.

By the end of the 20th century Distributed Temperature Sensing (DTS) consoles based on this principle were widely available, though applications were limited and resolution was poor (Feced et al. 1997). The first documented and peer-reviewed use of DTS in stand-alone hydrological applications was by Selker et al. (2006), who conducted a series of pioneering field experiments and revealed vast improvements in spatial, temporal and temperature resolution. In an experiment measuring stratification in a flooded mine shaft they reported a spatial resolution of approximately 1m with temperature resolved to 0.01 ˚C. They also identified trade-offs between these parameters; high spatial resolution results in fewer scattered

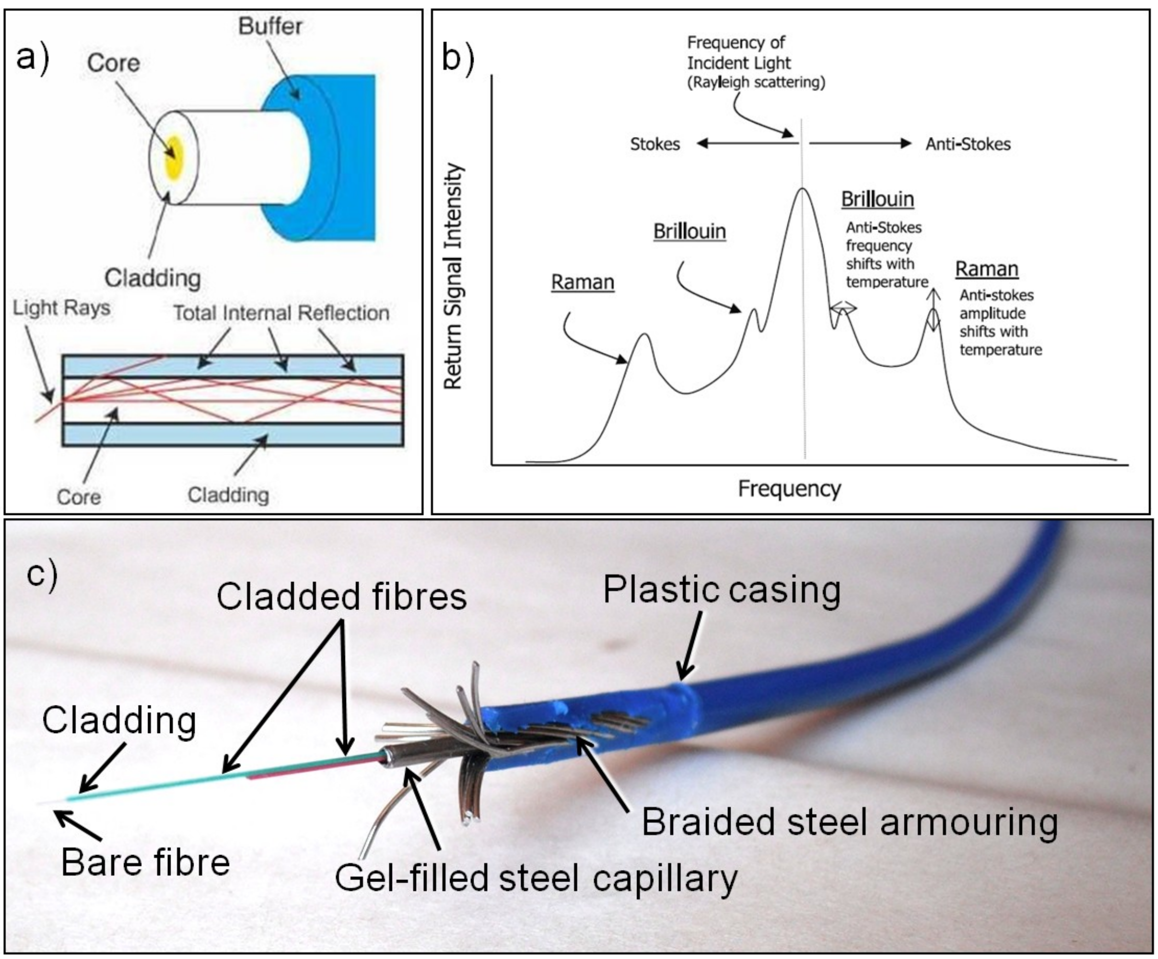

Figure 2 a) A schematic of fibre-optic cable and light propagation. Source: EW Blogs, 2011. b)Frequency distribution of scattered laser light in the DTS cable. Source: Selker et al. 2006. c) Photo of the 4 mm cable used in this experiment, stripped so that all layers are visible.

photons per unit length, requiring a longer integration time to provide a precise temperature. Tyler et al. (2009) elaborated on these trade-offs and investigated repeatability, resolution, and instrument options. Tyler et al. also discuss in detail considerations for field deployments and recommend certain calibration and data verification techniques including the use of a fixed-temperature reference such as an ice bath.

DTS has since been used in numerous hydrological applications, each one combining an established technique and previous findings to improve methodology, test its robustness, and gain further insight into the system being studied. Henderson et al. (2009) combined a 42-day DTS deployment with wavelet analysis to investigate submarine groundwater discharge (SGD) into Waquiot Bay, Massachusetts. Using a single transect perpendicular to shore they found that temperature changes within 13 m of shore were dominated by tidal influences while further out the diurnal signal dominates. They also detected a cold anomaly previously identified as a region of SGD (Michael et al. 2003), demonstrating that DTS can be used to make inferences about hydrologic structure and processes. Lowry et al. (2007) used DTS to identify preferential groundwater pathways entering a peatland spring in Wisconsin, first exploring the use of temperature variance (or standard deviation) as a means of identifying groundwater inputs. Moffett et al. (2008) experimented with a very short (32 hour) DTS deployment in a California salt marsh, finding that infiltrated warm tidal water re-emerges and keeps surface water consistently warm. They also showed that very small tributaries hidden by vegetation facilitate mixing between ground water and surface water. Slater et al. (2010) successfully used DTS to verify that differences in lithology inferred with continuous waterborne electrical imaging were relevant to GW/SW interactions in the Columbia River near a contaminated site. Nielson et al. (2010) used thermistors and DTS to measure the effect of direct solar heating and bed conduction on DTS cable, showing that DTS cable in shallow, clear water is subject to heating not related to water temperature. Briggs et al. (2011) quantified groundwater flux through a streambed with high-resolution DTS data. They used DTS first to find focused groundwater flow and then, with a mixing model, used the temperature data to calculate the rate of that flow. Very recently, Striegl and Loheide (2012) used DTS to estimate soil moisture by simultaneously measuring temperature and producing heat with resistance heating elements which were built into the DTS cable. They found that DTS was useful for measuring soil moisture in relatively dry conditions, but reported difficulties with instrument sensitivity to ambient temperature and relative humidity which caused data to be compromised and subsequently discarded.

The purpose of this study is to use DTS and other temperature-based methods to draw inferences about the hydrogeologic processes influencing SGD along a section of the shoreline at Indian River Bay, Delaware. DTS data are compared to previously acquired geophysical and seepage meter data in order to evaluate the effect of overlying sediment on groundwater discharge paths and fluxes. Implications for local and regional groundwater - surface water exchanges are discussed. Finally, field considerations for DTS use are described, and methods for processing, exploring and interpreting DTS data are elaborated.

Study Site

Holts Landing State Park, located on the south shore of Indian River Bay, Delaware, is surrounded by agricultural land and, along the shore, mainly seasonal (summer) housing. The bay, like many other inland bays on the Delmarva Peninsula (Figure 3) experiences symptoms of eutrophication such as seasonal phytoplankton blooms associated with nutrient-rich runoff and submarine groundwater discharge (Andres, 1991; Andres, 1992; Cerco and Seitzinger 1997; Dillow and Greene, 1999). In particular, elevated nitrogen levels have been detected throughout the region's groundwater system and are believed to be associated with fertilizer application, intense poultry farming and residential sewage (Andres, 1991; Andres, 1992; Denver et al. 2004). Cerco et al. (1994) provide an accounting of the water flows and nutrient loads to the bay, although these are likely out of date due to residential development and changes to regulations and practices (Alexander et al. 1999).

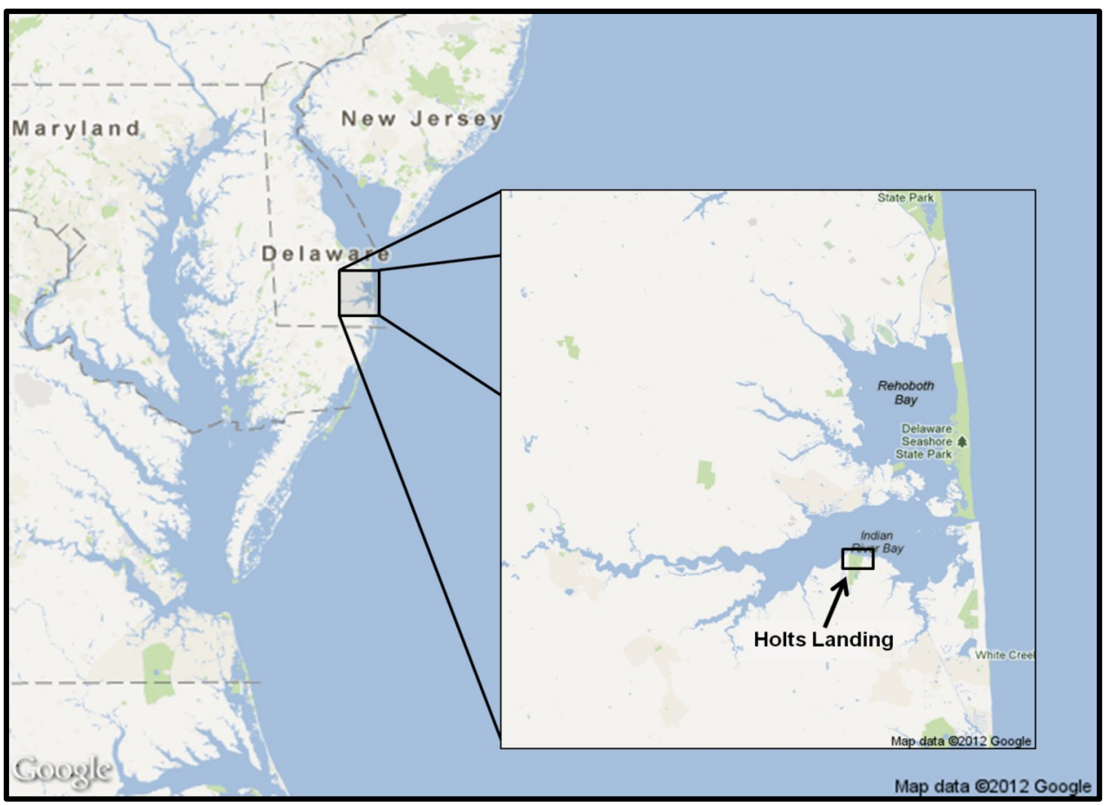

Figure 3 Map of the Delmarva Peninsula and Holts Landing State Park. Source: Google Maps

Indian River Bay is connected to Rehoboth Bay, and both are separated from the Atlantic Ocean by spits which are part of the barrier island system extending down the east coast of the USA (Figure 3, inset). The bays are linked to the ocean via an outlet that is only about 150m wide, restricting water exchange and resulting in a back-barrier situation where nutrient-rich sediment transported from the uplands is deposited in the brackish estuary (Oertel, 1985). Indian River Bay is approximately 15 m deep at its centre and reaches 25 m depth near its prehistoric outlet, which is now blocked by a spit (Krantz et al. 2004). Residence time in the bay is not well constrained, with estimates from one author ranging from 1.2 to 174 days based on tidal flushing and freshwater flows, respectively (Cerco et al. 1994). The tidal period in the bay is semi-diurnal, with a frequency of approximately 1.9 day $^{-1}$. Water levels for the duration of the current study's field work are presented in Figure 4.

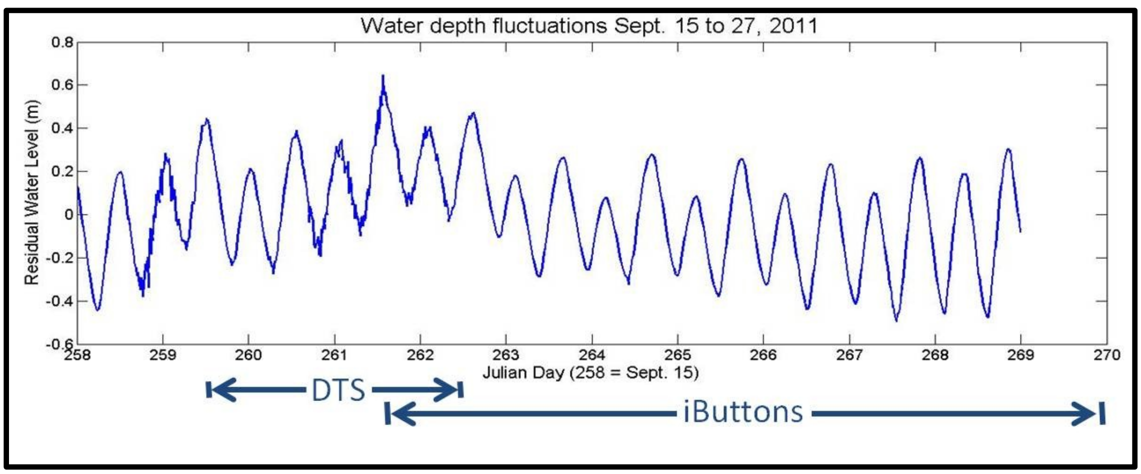

Figure 4 Sea level at Holts Landing September 17–20, 2011. Values are relative to the September 15-26 mean, and were measured with an In-Situ inc. AquaTroll 200 Conductivity, Temperature and Depth (CTD) logger. Bars below the figure indicate the duration of DTS and iButton deployments.

The geological setting of Indian River Bay has, at least since the Miocene, been shaped by its coastal location and alternating high and low sea levels. The bay is a relict of the lower reaches of the Indian River, which incised the coastal plain as it drained continental glacier meltwater (Cerco et al. 1994). The fine deltaic sediments of the Miocene Bethany formation act as a confining layer below the regional surface Columbia aquifer, which is made up of the late Pliocene to Pleistocene Omar and

Beaverdam formations (Groot et al. 1990). These upper formations are approximately 30 m thick at Indian River Bay, and are quite heterogeneous, consisting of interbedded estuarine and lagoonal clayey silts to gravelly coarse sands atop fluvial-deltaic coarse sands and gravels. The Beaverdam formation fines upwards and at Holts Landing the top of the formation, located about 13 m below the sediment/water interface, is believed to be a local semi-confining layer (Groot et al. 1990; Krantz et al. 2004). Holocene deposits vary across the bay, but tend to be finer organic-rich sediments which cap a thin layer of sand. A coordinated

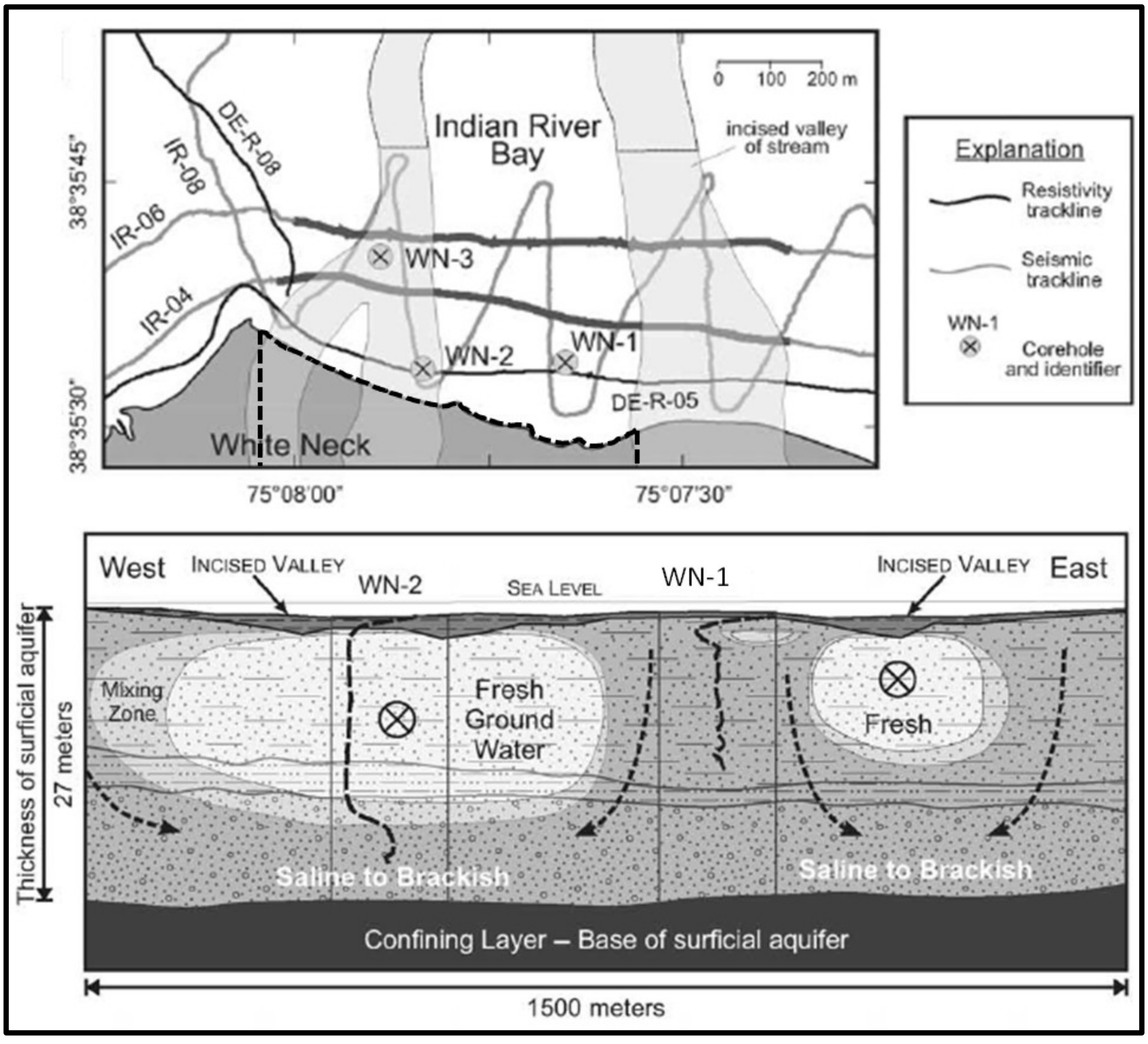

Figure 5 Top: Geophysics results suggest the presence of shallow, peat-filled incised valleys (shaded areas) on either side of Holts Landing (dashed line). Bottom: Cross-section of the Columbia aquifer underneath and between the channels, interpreted from resistivity and seismic data. Dashed lines at WN-1 and WN-2 indicate relative EM induction conductivity. Low values are to the left. Modified from Krantz et al. 2004.

geophysical assessment of Indian River Bay in 2004 revealed a dendritic network of submerged valleys which were formed by ancient tributaries to the Indian River system (Krantz et al. 2004, Manheim et al. 2004). These shallow (2 to 3 m) valleys, including one on either side of Holt's Landing (Figure), are infilled with sand and peat and topped with a thin layer of low-permeability mud from the tidal creeks and marshes that lie upstream. They are believed to act as preferential flow paths which route tongues of fresh groundwater under the mud and towards the centre of the bay (Krantz et al. 2004, Manheim et al. 2004) although, in general, how the local groundwater system interacts with the bay is not well understood (Bratton et al. 2004).

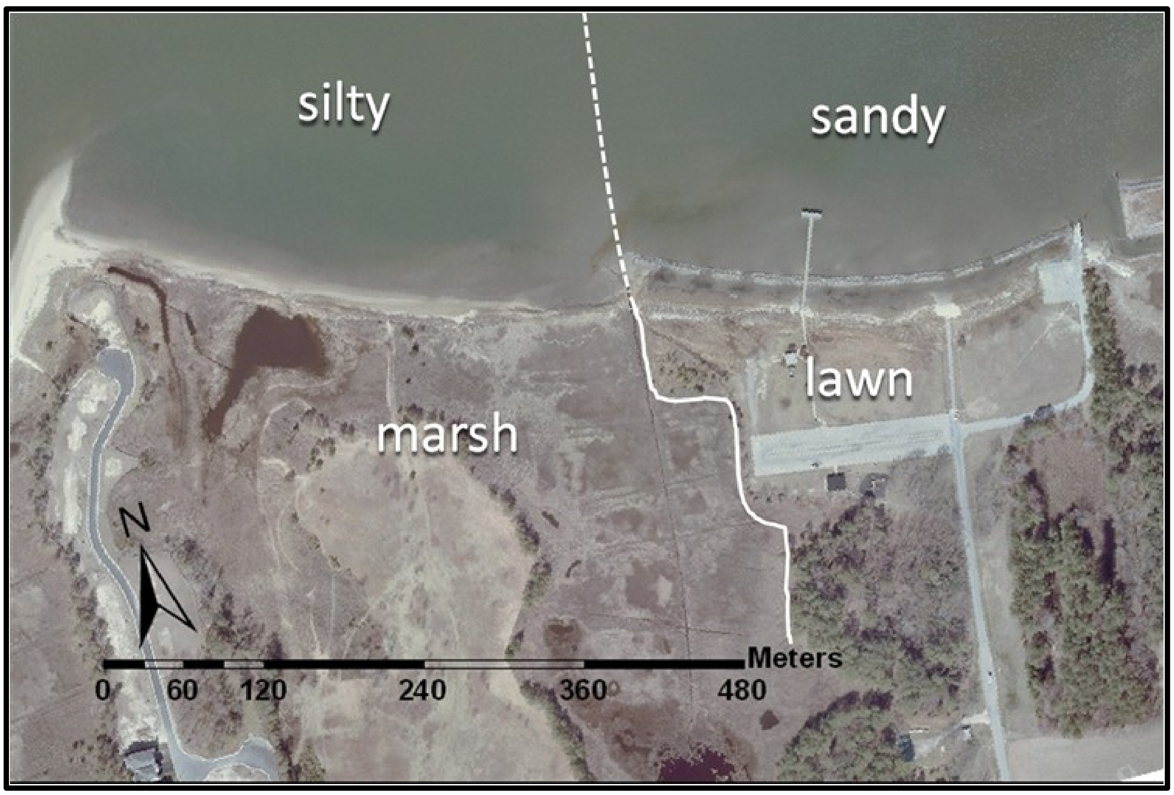

Figure 6 Orthophoto of Holts Landing State Park. The west side is dominated by marsh-derived silts and muds, while the east side is sandy. Source: Delaware Geological Survey

The land surface at the west side of Holts Landing is tidal marsh, which, moving eastward, changes suddenly to a slightly elevated sandy, managed lawn area (Figure 6). While the tidal marsh grades gently into the bay, the park lawn is separated from the water by a narrow strip of scrub which sits atop a steep embankment approximately 1.5m tall. This erodible face is protected from the bay by riprap breakers which extend above the water surface even during high tide. The breakers terminate in the east near a boat ramp which also marks the eastern edge of the park. Beyond the boat ramp a marina entrance, constructed in approximately 1957, interrupts the shoreline. The bay floor in the area is very flat, with a bayward slope of less than 0.4%, and it exhibits a clear shift from sandy to silty sediment towards the westward marsh zone.

CONCURRENT STUDIES

Russoniello et al. (in preparation) used a combination of geophysical and hydrogeologic methods to characterize porewater salinity and SGD in Indian River Bay near Holts Landing in 2010 and 2011. Chirp seismic and continuous resistivity profiling were used to investigate geology and salinity over kilometres, while Lee-type seepage meters and porewater sampling provided information on SGD and salinity at local scales. Their research produced over 550 seepage meter measurements near Holts Landing, providing information on flux and salinity. Results became available after the field deployment and are referenced here for comparison.

Methods

DTS DEPLOYMENT

Field work was conducted at Holts Landing from the evening of Friday, September 16, 2011 through Monday morning, September 19, 2011. During this time, temperatures at the sediment/water interface on the bay floor were measured using a DTS system (Figure) comprising a laser light transmitter/receiver console (Agilent / AP Sensing N4386A), a laptop computer to control the console and save data, and approximately 2000 m of double-stranded fibre-optic line (Brugg Brusteel 2FGS). The fibre-optic cable was laid out in zig-zag fashion approximately parallel to shore in order to detect east-west differences due to the presence of the western paleochannel indicated in Figure . Each of these limbs was approximately 420 m long, and located between 10 and 130 m from shore. DTS deployment was conducted in five stages, comprised of line preparation, route planning, cable emplacement, console and control setup and, finally, georeferencing. Since there is little in the literature about these steps and their implications for fieldwork, they will be covered in detail here.

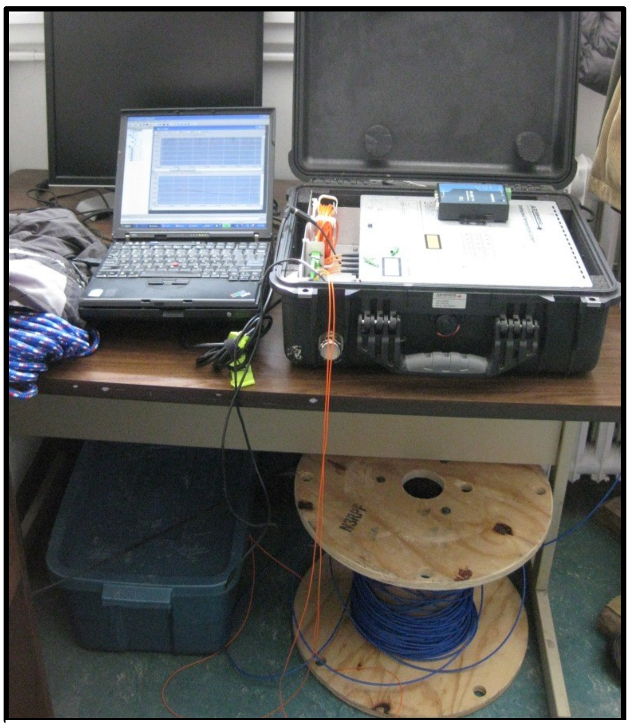

Figure 7 DTS apparatus in lab with laptop computer and a test spool of fibre optic cable.

Cable preparation

At one end of the cable, each of the two fibres was fused to a lead which could be connected to the console with an E2000 connector. At the other end, the fibres were joined using a Fujikura Splice Mate fusion splicer, providing a total fibre length of 4046 m. A segment of braided steel in the cable next to the splice was exposed and then splayed. The entire splice and splayed cable end were inserted into a plastic bottle which was subsequently filled with cement and sealed with polyurethane construction adhesive. This served not only to protect the splice, but also acted as a grippable, heavy handle which made cable deployment and anchoring easier. Noise tests of the splice showed a loss of 0.5 dB, or about 8% of the 6.5 dB loss along the full line. The cable was spooled onto a portable hand reel, with the leads on the inside protruding from the centre to allow connection to the console. The sealed spliced end sat on the outside of the spooled cable.

Route planning

Planning involved careful consideration of the desired cable layout, the amount of cable available, the physical obstacles that might be encountered, and infrastructure needs such as a power supply and protection from the elements. A preliminary map was sketched out indicating the areas of interest, a proposed route for the cable, and a careful estimate as to the amount of cable required. In this case, the DTS line needed to cross the pier twice, swing around a series of tall pilings in the nearshore zone, and terminate in a van near a state park outbuilding with electrical outlets (see Figure 8). Since it would have been impractical to drag nearly 2 km of line from this final location, it was decided to deploy cable from the pier and then manipulate the cable reel into its final location after most of the cable (and weight) was deployed. This meant that the cable reel would have to be lowered from the pier, carried underneath it, and moved onto shore and into the van through an open window. A failure to identify and plan for any one of these steps would have resulted in the need to retract the entire line, start over, and possibly rethink the plan entirely.

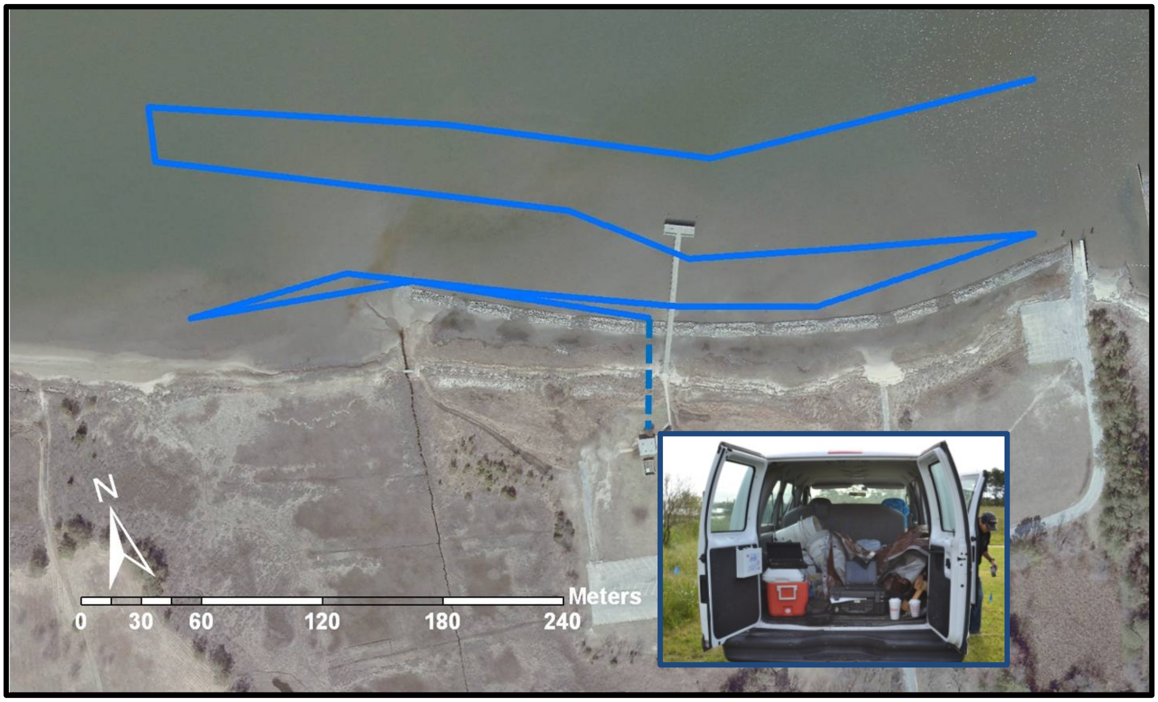

Figure 8 Fibre optic line was laid out approximately parallel to shore. The dashed segment was not submerged, and terminated at the console in a van near the outbuilding (inset).

Emplacement

Once a plan was established, the reel was placed on the pier, maximizing visibility of the field site while minimizing contact between the line and solid (drag-inducing) objects. The sealed, spliced cable end was pulled out and threaded through the pier pilings as necessary, making all of the turns it would have to make. It was then dragged out to its desired location at the far north eastern corner of the study area, and anchored with a Brugg line clamp attached to a metal spike which was pressed into the sediment. From there, the planned route was followed backwards, with the cable gradually being released from the reel and anchored in similar fashion at each corner. When most of the cable had been deployed the reel was moved to shore and into the van, where it could be secured.

Console setup

An important component of the DTS deployment is correcting for instrument drift and offset. Two loops were used for this purpose – one in a water-saturated ice bath and the other at air temperature. A control loop of approximately 12 metres of line was submerged in an ice bath in a cooler inside the van. Two iButton Thermochron temperature data loggers (Maxim-IC, Sunnyvale, CA) were taped to the loop in order to provide independent temperature measurements. Two other data loggers were placed in an insulated package at ground level outside the van.

The two cable leads were attached to the console, which was programmed to perform two sets of measurements at a one-metre spacing every 12 minutes: one four-minute ‘single-ended’ measurement and one eight-minute ‘double-ended’ measurement. Single-ended measurements are made from only one of the leads. Since noise is a function of distance from the controller, this provides a signal that degrades progressively away from the console. Double-ended measurements, on the other hand, reduce noise by alternating measurements between the two leads. Both types of measurements were taken as a means of comparing and exploring the resulting data quality. While that comparison is not within the scope of the current study, it is important to understand that the data presented below derive from the double-ended measurements.

Georeferencing

The DTS line was surveyed from the end of the pier with a Trimble S3 DR Series total station, which was in turn backsighted to a local Delaware Department of Transportation geobenchmark located in the park and fixed to the NADV 1929 datum. A total of 17 points were surveyed, primarily at bends in the line and in the middle of long, straight stretches. We employed two methods to determine what segment of line was represented at each point in the data file. The first relied on metre markings on the cable itself, which were read at each survey point. The second involved forming a small (2-3 metre) loop in the cable at each point and tucking it into the wetsuit of the person holding the prism. This resulted in a temperature anomaly which was visible real-time in the DTS output. The metre markings and display output distances were recorded simultaneously during the survey, compared, and then linearly interpolated to all points on the line.

DATA HANDLING

Since DTS measurements are subject to temporal drift and noise (Tyler et al. 2009), the measured data were corrected using the output of the two iButton temperature loggers submerged in the ice bath. The iButtons, accurate to 0.5 degrees, were programmed to measure temperature every 10 minutes at 0.0625 ˚C resolution. The iButton data were trimmed and resampled to match the DTS measurement times using MATLAB's linear *interp1* function. The two resulting datasets were averaged, providing a high-resolution, low-noise control for the submerged DTS loop. At the same time, the DTS output was visually assessed to locate the 12 m loop in the ice bath, and the data from the loop's central six meters were averaged to generate a DTS-derived ice bath mean at each timestep. The three metres on either side of this 'core' were ignored in order to minimize the chance that temperatures outside the ice bath were averaged into the control. A correction factor (CF) was created by subtracting the iButton mean from the DTS mean at each timestep. The DTS dataset was then corrected using

$$\text{Corrected DTS } (i, j) = \text{Raw DTS } (i, j) - \text{ CF}(i) \text{ ,}$$

where i and j represent time and space, respectively. See Appendix A for more details.

At one point the cable, which had been kinked during deployment, broke. The break was repaired in the field, but some data were compromised due to both the kink and the break. Two major blocks of data were discarded after a visual inspection of the output (see Figures 13 and 14), while the metres clearly affected by the kink were re-calculated as the mean of the previous five metres (for those closest to the console) and the following five metres (for the seaward side metre). These data were not used in further analyses, except to calculate statistics for the overall dataset. In order to reduce the temporal noise and smooth the corrected signal, the temperature reading at each metre was recalculated as the average of itself and the two timesteps preceding and following it. This was done twice. Values with less than two real-number neighbours before and after (for example, the first temperatures recorded or those next to the discarded data) were weighted more heavily in their own average. The script used to smooth the data can be found in Appendix B.

For visualization and spatial analysis, the corrected, smoothed, and georeferenced data were imported into ArcGIS. Here data were explored visually and then analyzed statistically in MATLAB. DTS analysis was limited to the section of line that remained continually submerged on the seaward side of the riprap breakers.

HATCH METHOD

Sediment and water column temperatures were also measured using four groups of four vertically-aligned iButtons which were mounted in recessed wooden stakes and inserted into the sediment (Figure). The iButtons were programmed to

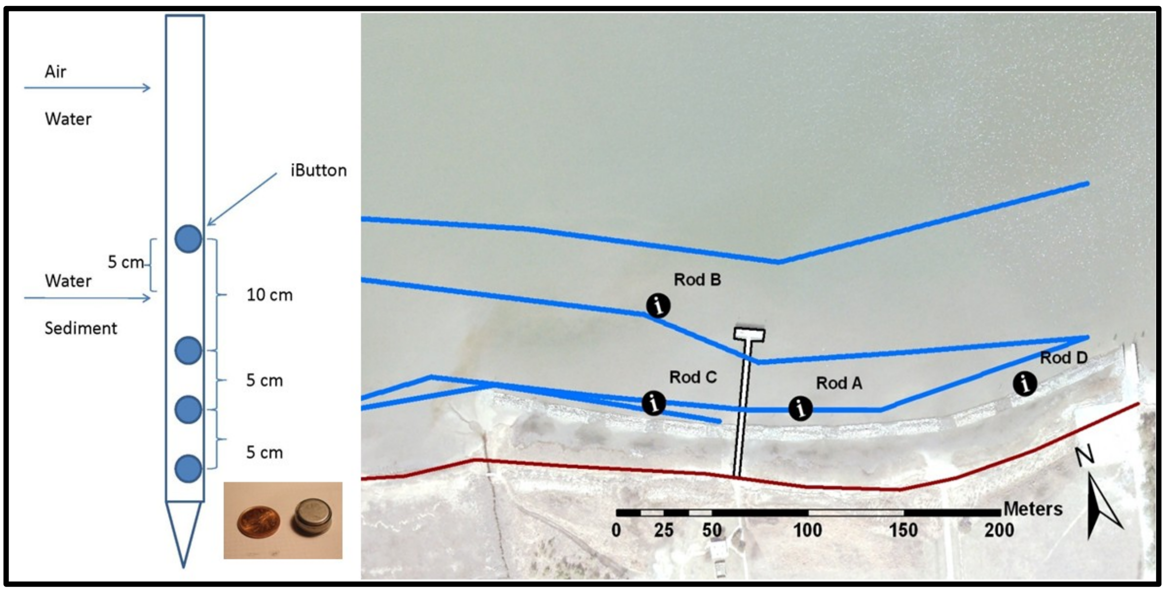

Figure 9 Design of iButton rod, built with a wooden stake and four iButtons (inset, with a penny for scale). Rod positions are shown relative to the DTS line (blue). The red line indicates the approximate shoreline.

record temperature every 10 minutes from September 18 to 27, 2011. The data were subsequently imported into MATLAB and assessed using the VFlux program (Gordon et al. 2012). VFlux automates the Hatch amplitude method (Hatch et al.2006), which solves for 1-D (vertical) water flux at a point based on a heat transport model populated with temperature data and physical properties of the water and sediment. The principle behind the model is that the diurnal temperature signal is attenuated with distance from the surface. Water flow into the sediment reduces attenuation since energy is transported along with the fluid. Flow out of the sediment increases attenuation (Figure 10). Therefore, the degree of attenuation can provide information on flux (q), which is calculated as

$$q = \frac{nC_w + (1-n)C_s}{C_w}\left(\frac{2\kappa_e}{\Delta z}\ln A_r + \sqrt{\frac{\alpha + \upsilon^2}{2}}\right),$$

where n is sediment porosity, C_w and C_s respectively are the heat capacity of the water and sediment, Δz is the distance between measurement points, υ is the thermal front velocity, and A_r is the ratio of the amplitude variation between the measurement points. κ_e and α are, respectively, thermal diffusivity, estimated as

$$\kappa_e = (\lambda_e / C) + \beta|q| ,$$

and

$$\alpha = \sqrt{\upsilon^4 + (8\pi\kappa_e / P)^2} ,$$

where P is the period, in seconds, of the temperature signal. Details on the solution are elaborated by Hatch et al. (2006).

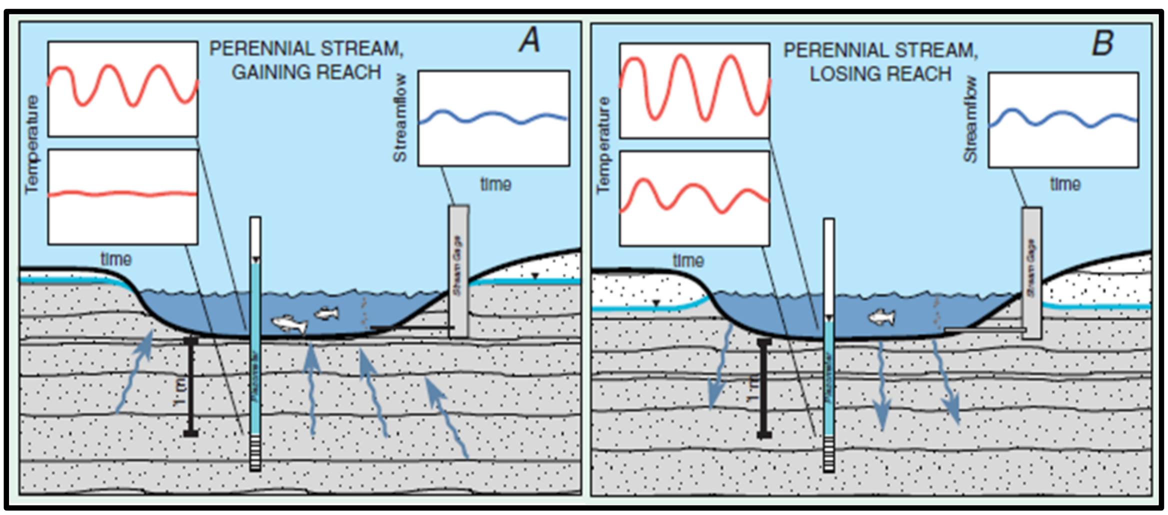

Figure 10 The Hatch Method uses the ratio of temperature signal amplitudes at different depths to calculate vertical groundwater flux. The gaining stream (left) will have a greater amplitude difference than the losing stream (right), where surface heat is carried downwards by flowing water. Source: Stonestrom and Constantz, 2003.

The model requires that three assumptions are met, namely that water flow is completely vertical, the dominant temperature signal (typically diurnal) is sinusoidal, and that sediment temperature is not depth-dependent. However, semi-vertical flow combined with non-sinusoidal temperature signals can reliably provide flux estimates to within an order of magnitude (Lautz, 2010). VFlux uses low- and high-pass filters on the temperature signal to provide the model with a noise- and trend-free sinusoidal input, thereby 'cleaning' the natural signal before processing.

Results

OVERALL AIR AND WATER TEMPERATURES

Air temperatures during the deployment were heavily influenced by Hurricane Maria, whose fringing systems produced rain and cool temperatures along the Delaware coast from September 16 to 19 (Figure 11). Groundwater temperature is estimated at 15.7˚C based on an extrapolation of data measured at 8m below the bay sediment in August 2011 using a CTD logger (Figure 12). Water temperatures at the sediment/water interface during the DTS deployment (Figure 13) ranged from 15.6˚C to 21.7˚C, averaging 17.8˚C. Processed data is presented in Figure 14.

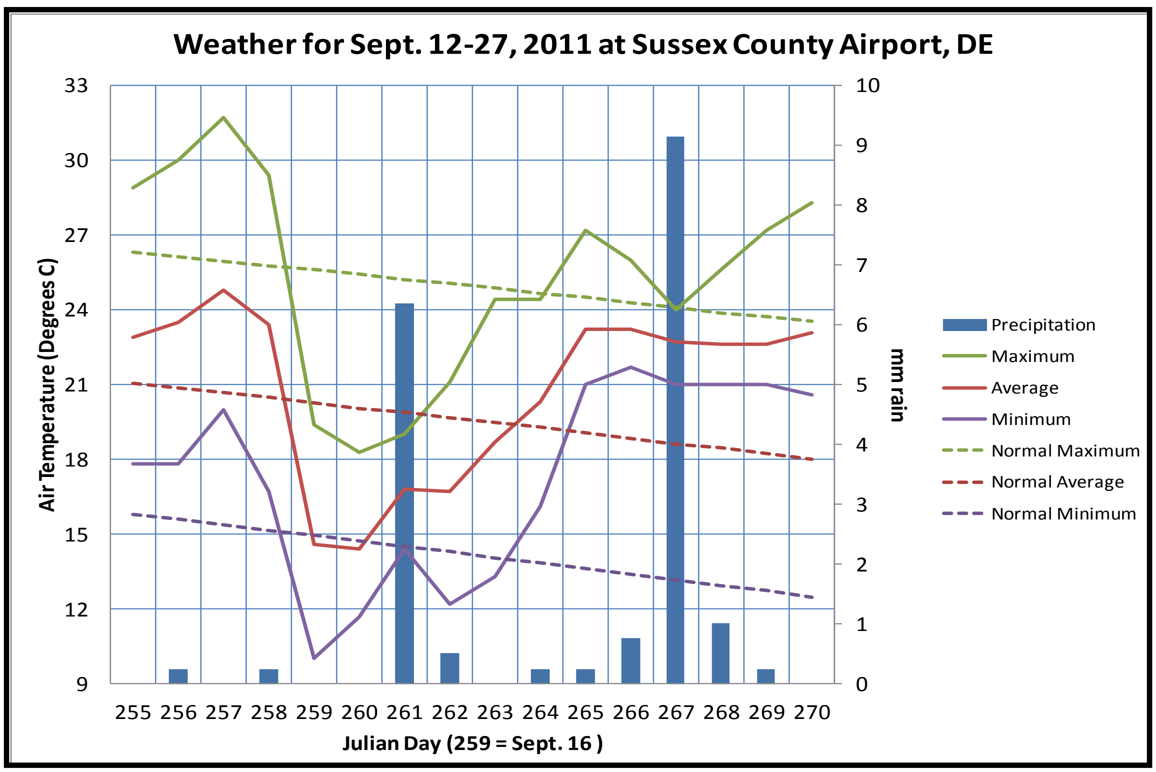

Figure 11 The DTS system was deployed on September 16, just as temperatures dropped suddenly below seasonal normals. It was removed on the morning of September 19 (Julian day 262) before temperatures recovered. iButton rods were installed on September 18 and retrieved on September 27, measuring a period with ample warming and precipitation. Source: NCDC (2012).

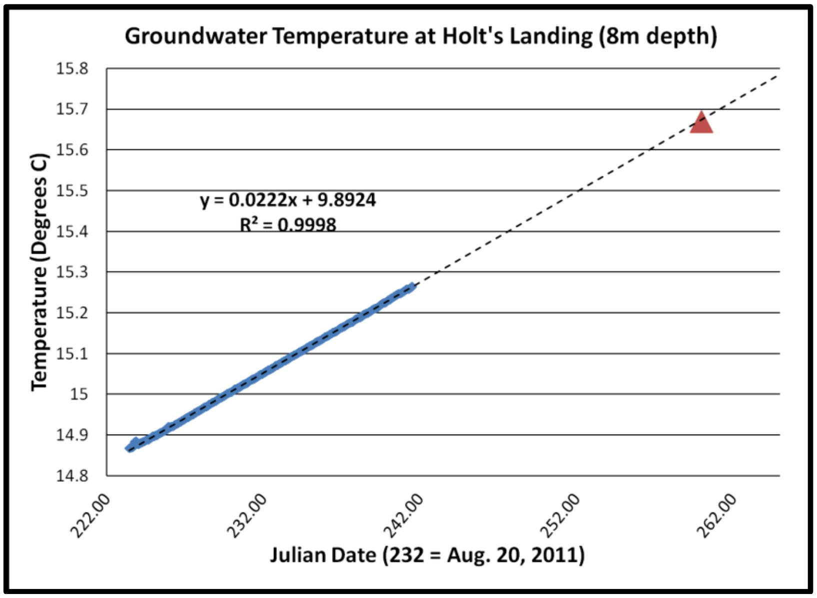

Figure 12 Groundwater temperatures were estimated to be approximately 15.7˚C (red triangle), based on an extrapolation of temperature data (blue) obtained for August 10-29, 2011.

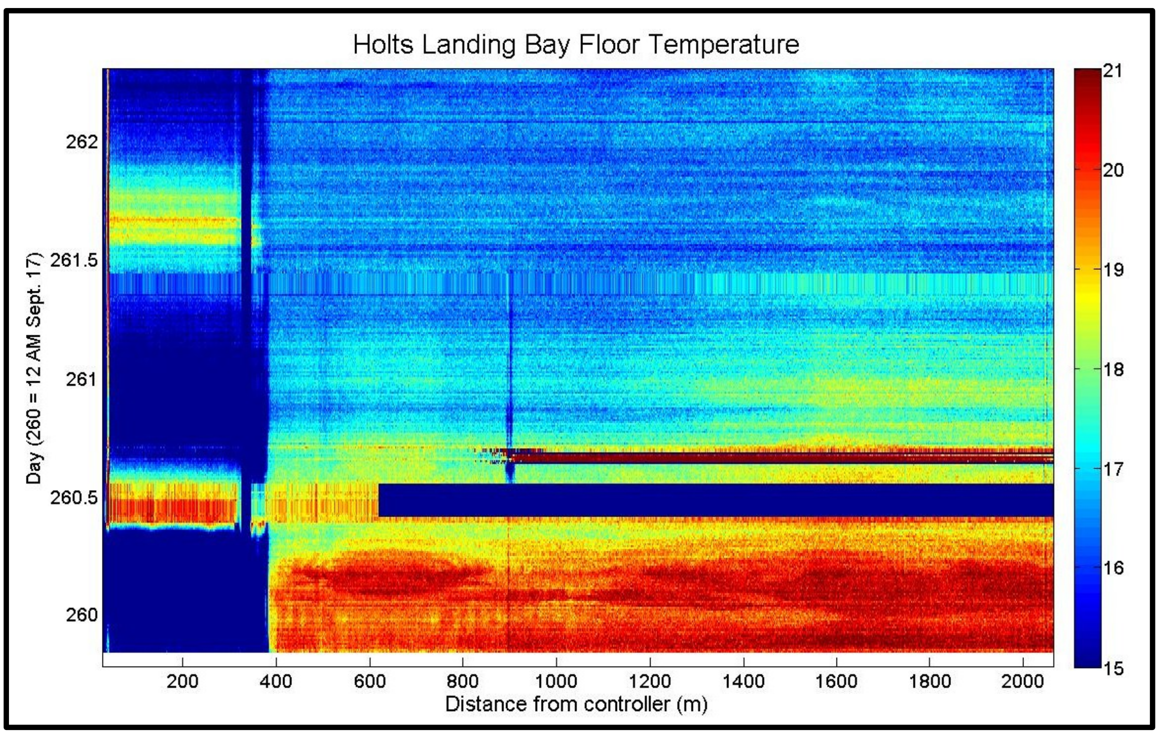

Figure 13 Raw DTS output, with temperature (˚C) represented by color. The large horizontal cool block at day 260.5 was caused by a line break, while the thinner warm block at day 260.7 appears to have been caused by stress on the repair splice at metre 890. The ice bath appears as a solid dark blue vertical line at metre 340.

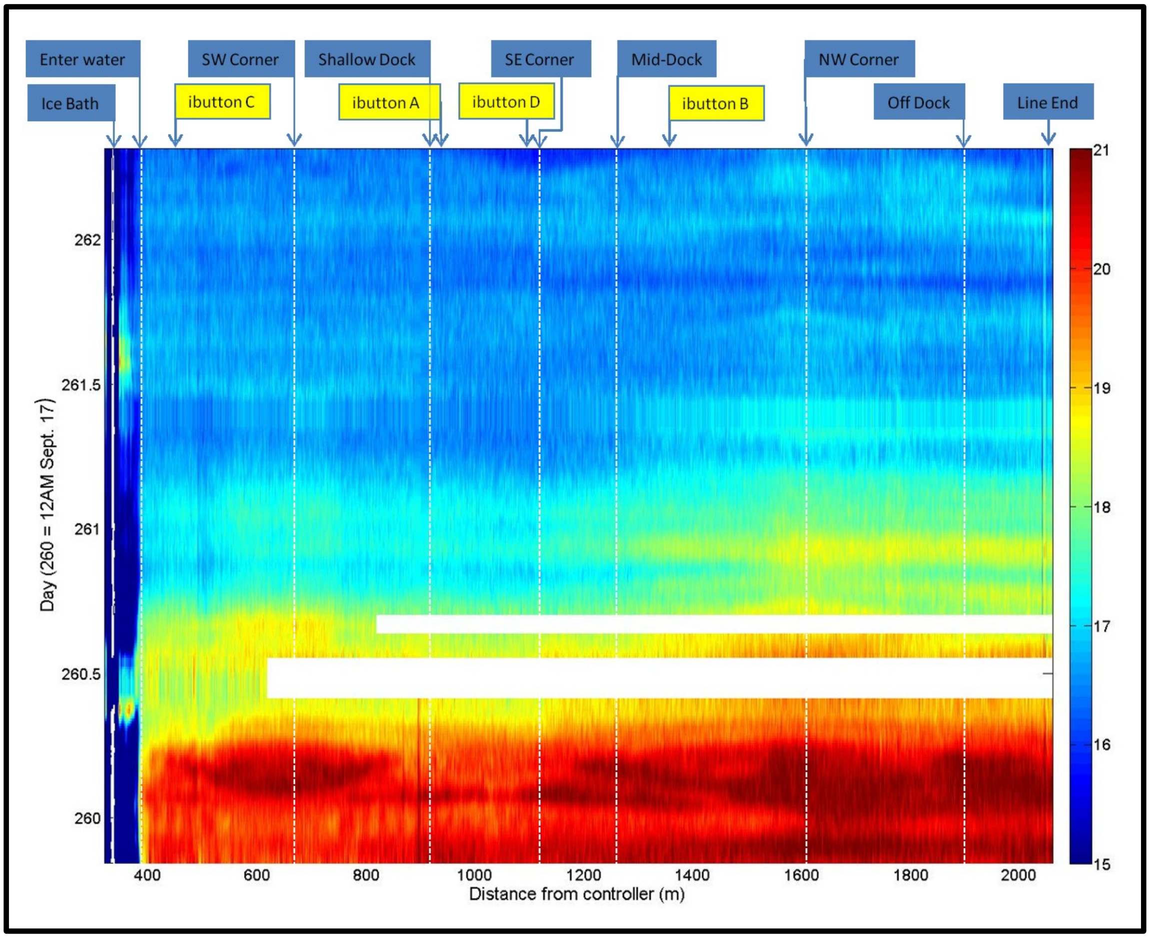

Figure 14 Corrected, trimmed and smoothed DTS data, with temperature (°C) represented by color. Locations of various landmarks with respect to the DTS cable are indicated at the top.

DTS – SPATIAL PATTERNS

The length of cable that remained continually submerged on the seaward side of the breakers was 1634 m. The minimum distance to shore (red line in Figure 1) for each point on the DTS line was calculated using the 'Near' function in the ArcMAP Analysis Tools Proximity toolbox, which calculates the shortest distance between two features. Temperatures were, on average, warmer further from shore. The best fit achieved using MATLAB suggests that, locally, temperature variance (s^2) increases with distance from shore (d) following the power function

$$s^2 = -33.63(d^{-1.012}) + 2.685$$

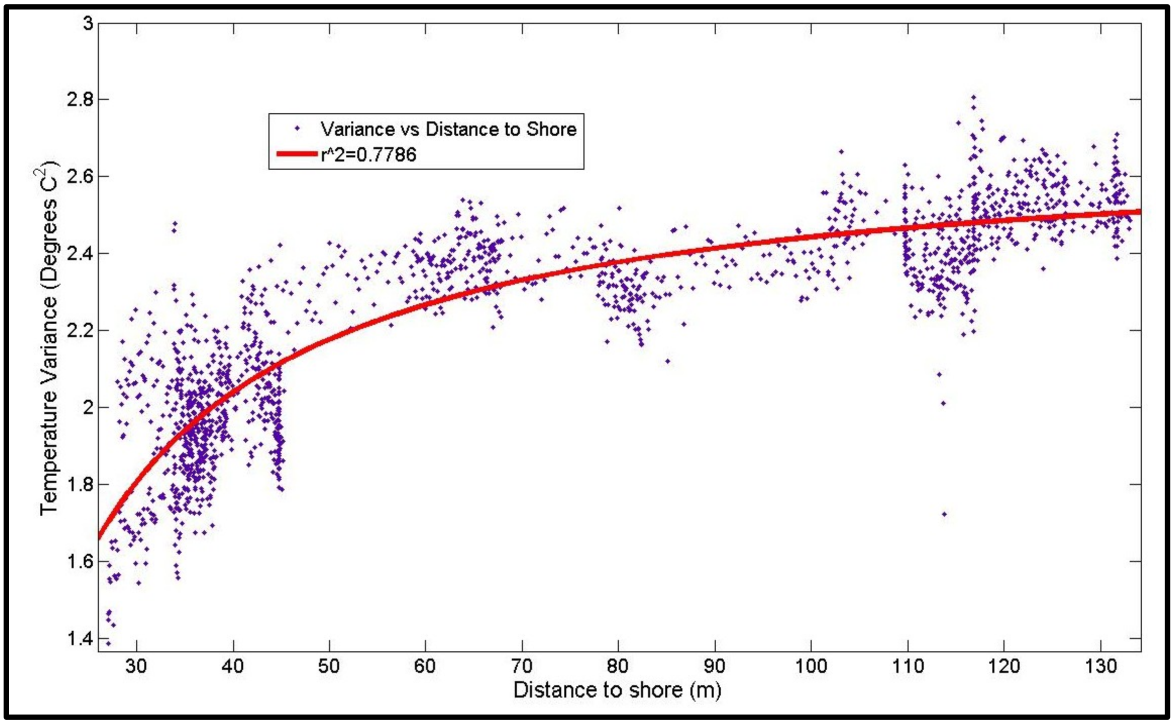

Figure 15 Temperature variance as a function of distance to shore.

(Figure). This trend was subtracted from the variance data in order to better resolve patterns along the east-west axis. Variance was also tested for its relationship to water depth, which is related to distance from shore, and can have implications for top-down heating and cooling. The coefficient of determination was for this relationship was weaker (r^2=0.67).

Finally, the possibility that variance is dependent on absolute temperature was eliminated by calculating mean temperature and standard deviation across a 9-meter sliding window for each data point, and plotting them together. The four values at each edge were ignored. The very poor coefficient of determination (r^2=0.04) indicates no significant relationship.

Mean temperature and variance were heterogeneous across the cable, with some distinct zoning (Figures 16 to 18). In the first 1000 metres of cable, two temperature zones stand out from the background. The first, a 10-metre band around the 500 m mark, appears cooler than its surroundings. The second, a wide band between 575 and 750m, exhibits consistently higher temperatures for the first day and a half and almost appears as a rectangle on Figure 14. On the half of the cable furthest from the console, there is a slightly cooler region (mean temperature approximately 17.6˚C) between 1000 and 1100 m and then a distinct warm band (mean temperature 18.1˚C) between about 1550 and 1760 m.

In terms of variance, the southwestern edge of the cable (618 to 660 m) experienced relatively high temperature variation, as did the area around the dock (900 to 1010 m and 1280 to 1320 m) and at the eastern near-shore extreme (1100 to 1130 m). Relatively low variances were observed in a swath between the dock and the western edge, in a 27-m segment near the shore close to the eastern edge (meters 1018 to 1045), and in a very narrow zone from 490 to 497 m. Very localized spikes in variance at 890 and 1742 meters were associated with observable kinks in the DTS line, the former being the location of the eventual break. Between 12 and 8 metres from the end of the line, consistently high temperatures were recorded, resulting in a lower variance.

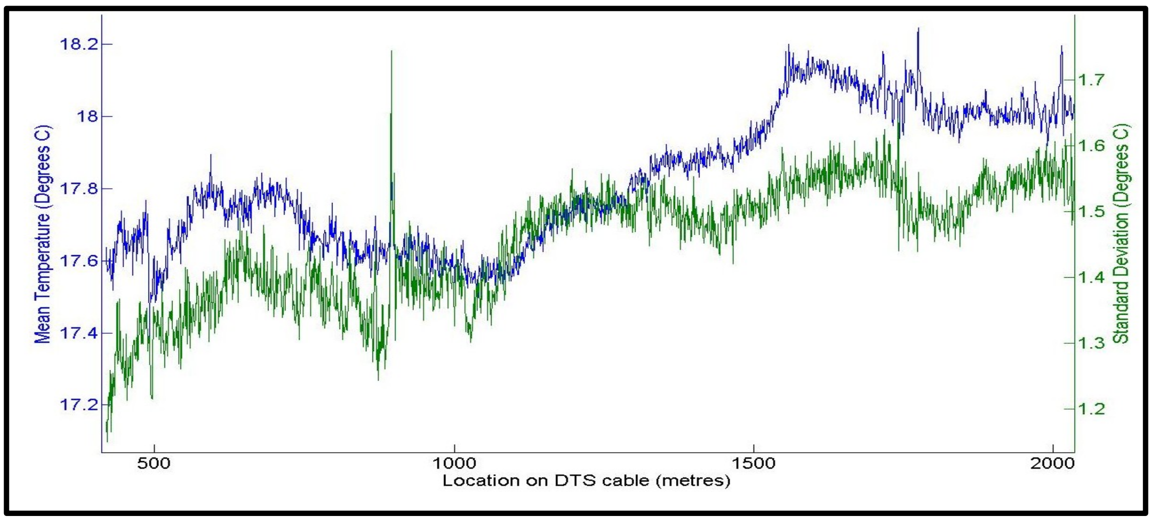

Figure 16 Temperature mean and standard deviation for each submerged metre of DTS cable.

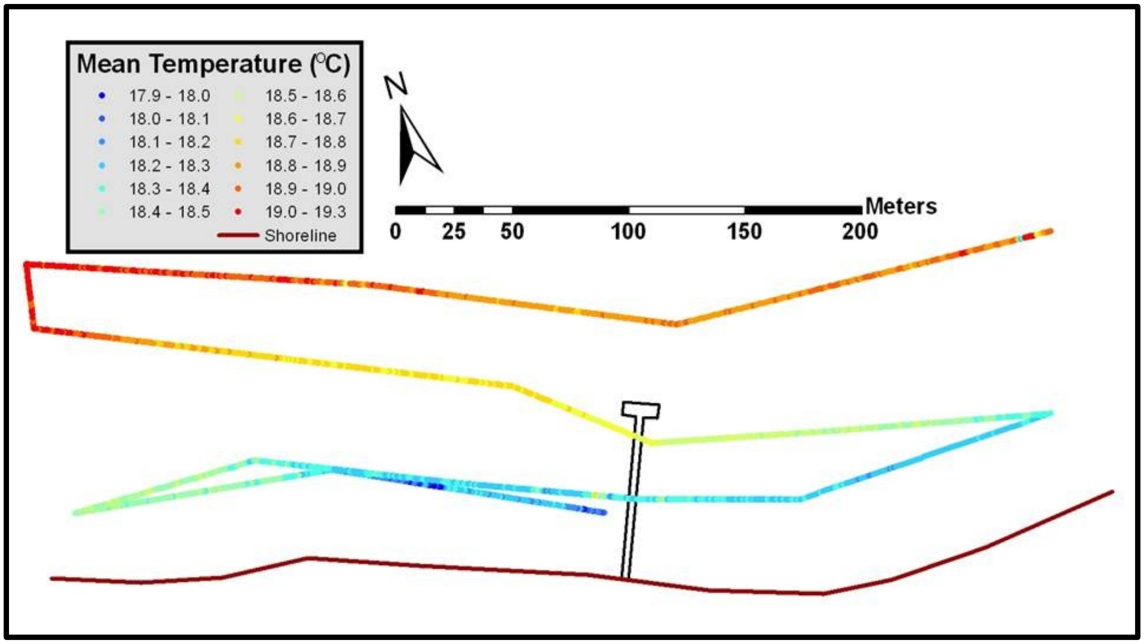

Figure 17 Map of the mean of temperatures measured from 8:15 PM September 16 to 7:20 AM, September 18 (see DTS Temporal Patterns below).

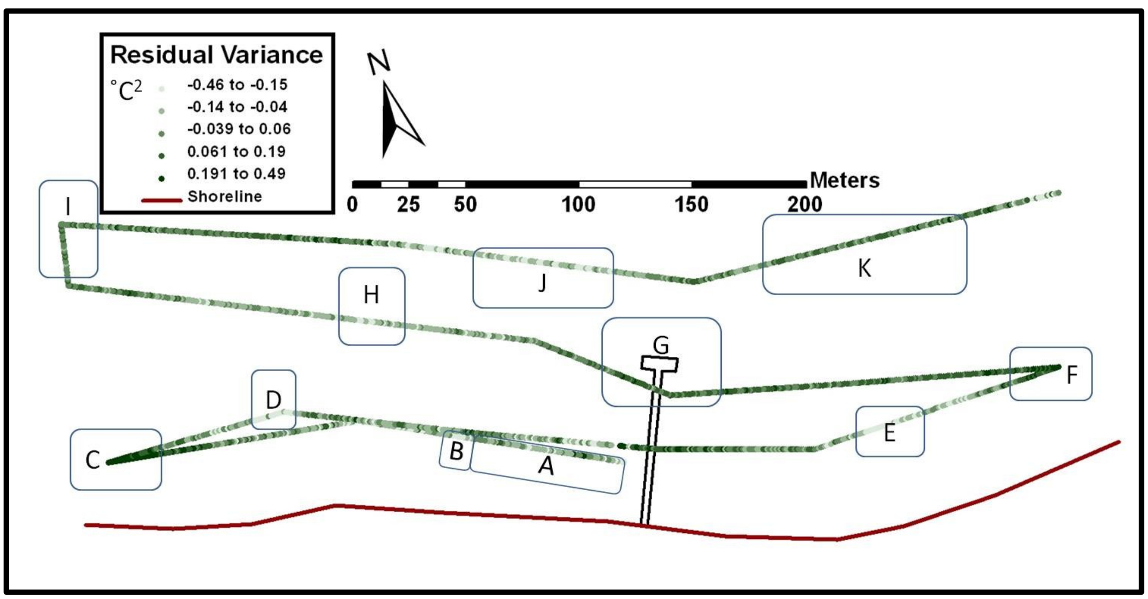

Figure 18 Map of variance, corrected for distance from shore (red line). Light areas along the DTS cable indicate relatively low variance. The zones indicated here were selected for comparison based on variance and mean temperature data.

Zones which stood out due to variance, mean temperature, or both were selected for further analysis (B to J, Table 1). Two other large zones that appeared relatively unremarkable (A and K) were also selected. Differences between zones were detected using the non-parametric Friedman's test on the mean temperature within each zone, blocked by measurement time, and quantified post-hoc with Tukey's HSD criterion ($p<0.05$). Temperatures measured after 7:20 AM on September 18 were deemed to have become homogeneous, likely due to the hurricane's influence, so were therefore excluded from this analysis. Differences in variance were tested using the Kruskal-Wallis procedure, then isolated using the same Tukey test. Results are summarized in Figure . Data collected during the two problem periods on September 17 were excluded from both analyses.

Table 1: Zones of interest based on temperature mean or variance

Zone	Location on cable (m)		Field setting	Observation
	From	To		
A	420	480	Near shore, W. of dock	Unremarkable, near shore
B	490	497	Near shore, next to Zone A	Low variance
C	641	686	Near shore, S.W. corner	High variance and mean
D	731	749	Near shore, at marsh margin	Low variance
E	1014	1047	Near shore, E. of dock	Low variance
F	1098	1132	Near shore, S.E. corner	High variance
G	1280	1326	Mid-dock	High variance
H	1428	1453	W. of mid-dock	Low variance
I	1584	1621	N.W. corner	High variance and mean
J	1798	1853	W. of dock, distant	Low variance
K	1920	2004	E. of dock, distant	Unremarkable, distal

Mean temperature data show that zone B is significantly cooler than zone A, which it abuts, and zone C, which lies just west in siltier sediment, exhibiting the highest temperatures of the nearshore zones. Zone I in the northwest corner is significantly warmer than any other zone. The variance comparison shows that zone

C and zone F, at the western and eastern extremes of the nearshore length, exhibit elevated variances. Zone G under and around the dock is nearly as variable. The swath of low variance observable just west of the dock is significantly different from the northwest corner as well as areas to the east, but, zone B, which appears as a narrow zone of low variance in Figure 18, cannot be shown to be less variable than neighbouring zone A.

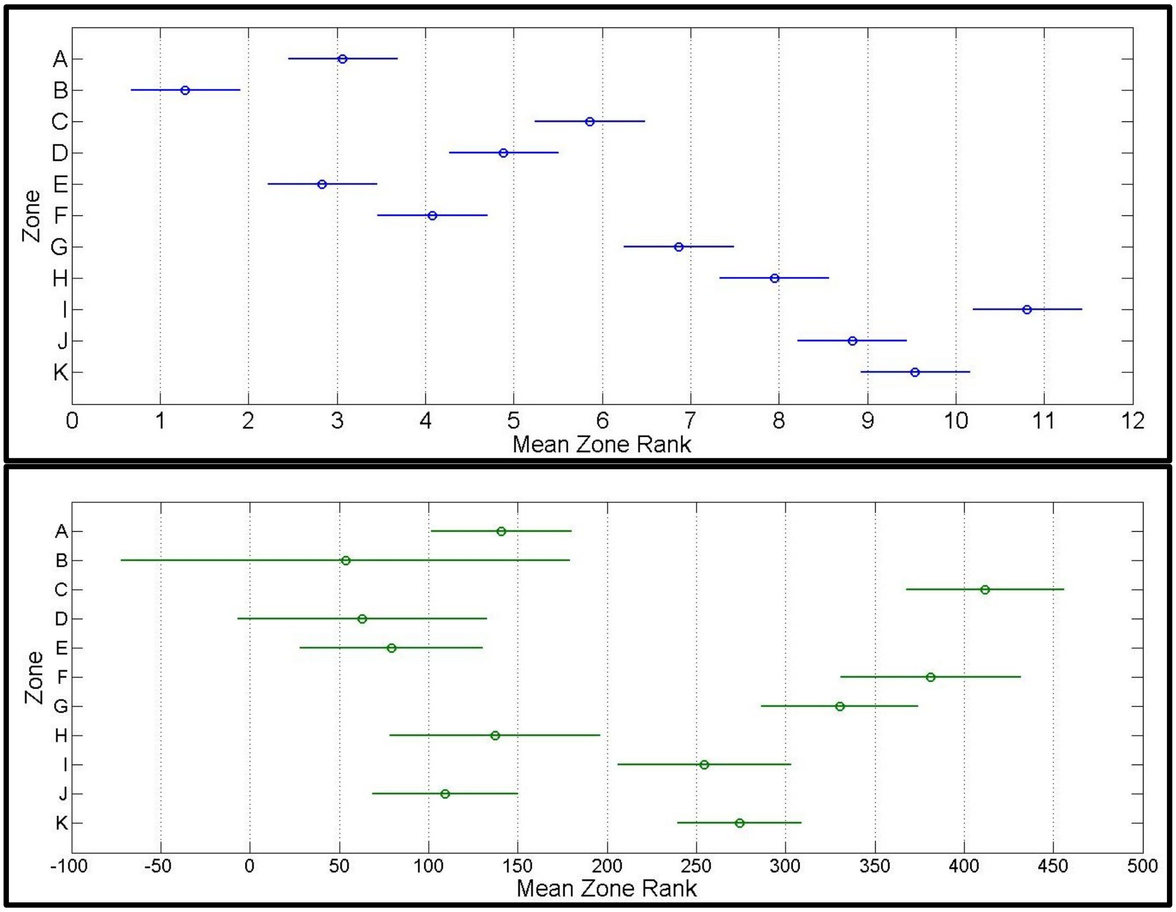

Figure 19 Each zone is compared to the others by using the zone's mean temperature (top) and variance (bottom). Zones are significantly different from one another ($p<0.05$) when their error bars are not vertically aligned.

DTS – TEMPORAL PATTERNS

In general, the water at Holts Landing became cooler and more uniform during the experiment, evolving to nearly homogeneous temperatures across the measurement area (Figures 14 and 20). The diurnal temperature signal observed in metres 350 to 400 of the cable is not detectable in the water except for a small rise in temperature in metres 400 to 600 just after noon on September 17. Some rapid changes in standard deviation and temperature do occur, most prominently at times I, II and III on Figure 20. These are discussed below.

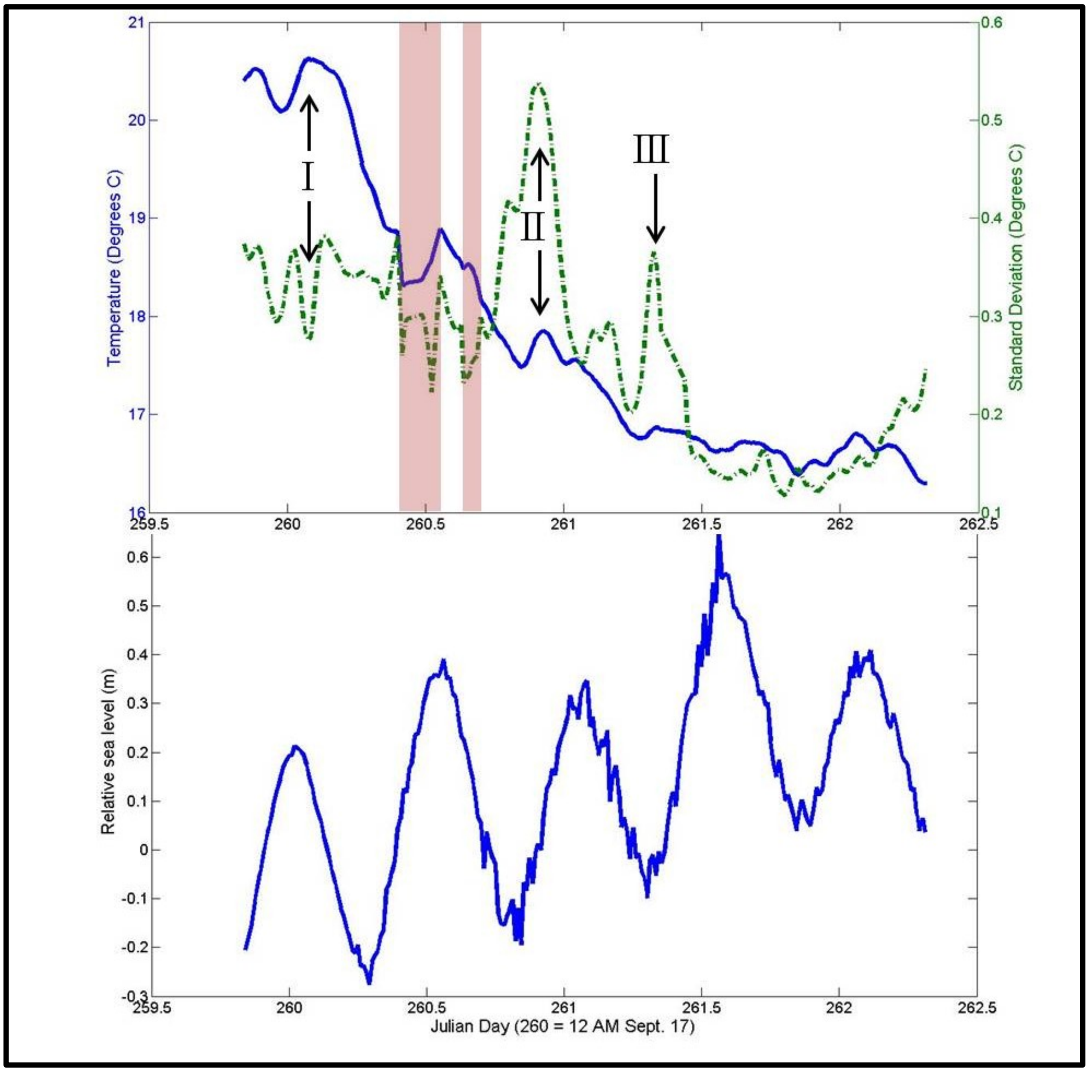

Figure 20 Top: Temperature mean and standard deviation for the entire DTS cable every 12 minutes. Shaded areas indicate times when data was compromised due to line damage. The phenomena at points I, II and III are discussed below. Bottom: Relative sea level at Holt's Landing September 17–20, 2011 (Extracted from Figure 4).

Time I

Time I in Figure 20 is characterised by an overall rise in temperature within the span of less than 2.5 hours, corresponding with a drop in standard deviation across the DTS cable, meaning that the cable became more uniformly warm during this period. It also occurred shortly after a tidal peak. In order to better understand the distribution and degree of the temperature changes, the trough-to-peak change in temperature for each metre on the cable was calculated by finding the minimum temperature from the two hours before the middle of the upslope in temperature and subtracting it from the maximum temperature in the following two hours. The average meter warmed 0.7˚C during this period. Most of the warming occurred shoreward of a sharp change near metre 1600, which is located in the northwest corner (Figure 21). Zones of above-average warming occur at 525 to 750m, 860 to 1020 m, 1085 to 1320 m, and 1450 to 1610 m.

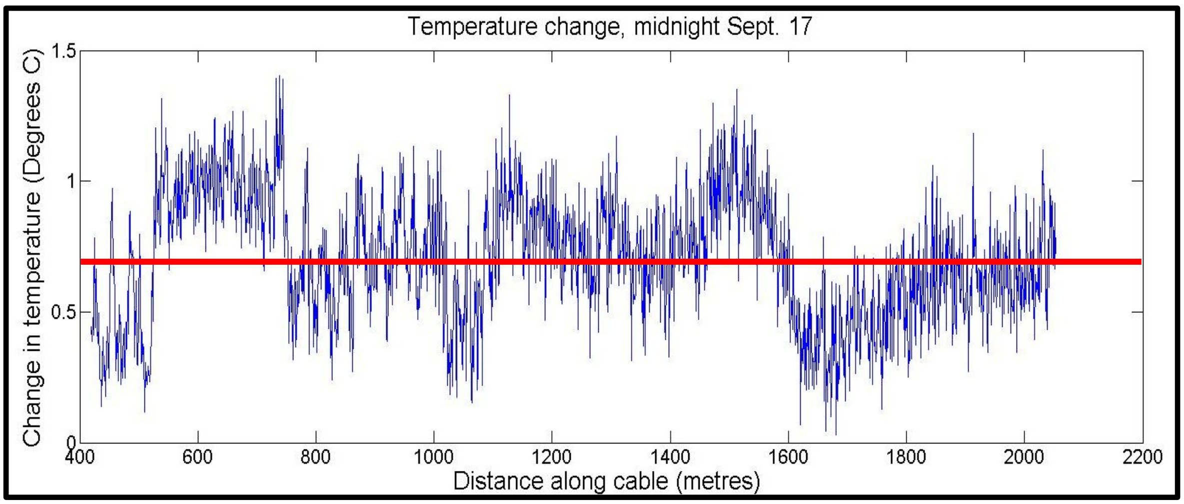

Figure 21 Change in temperature at each metre during the sudden warming beginning around 12 AM, September 17. The straight line indicates the average temperature increase.

Time II

At time II, there is a large, stepped spike in standard deviation accompanied by a small rise in mean temperature shortly following low tide. Local changes were isolated in the same way as for time I. For time II, warming was concentrated between 1250 to 1400 m and 1800 m to the end of the line (Figure 22). These coincide with segments of the line located at the mid-dock (Zone G above) and north and east of it. The behaviour of the temperature at the far end of the cable is notable around this time, warming briefly while the rest of the line cools, and contributing to the step in standard deviation (Figure 23).

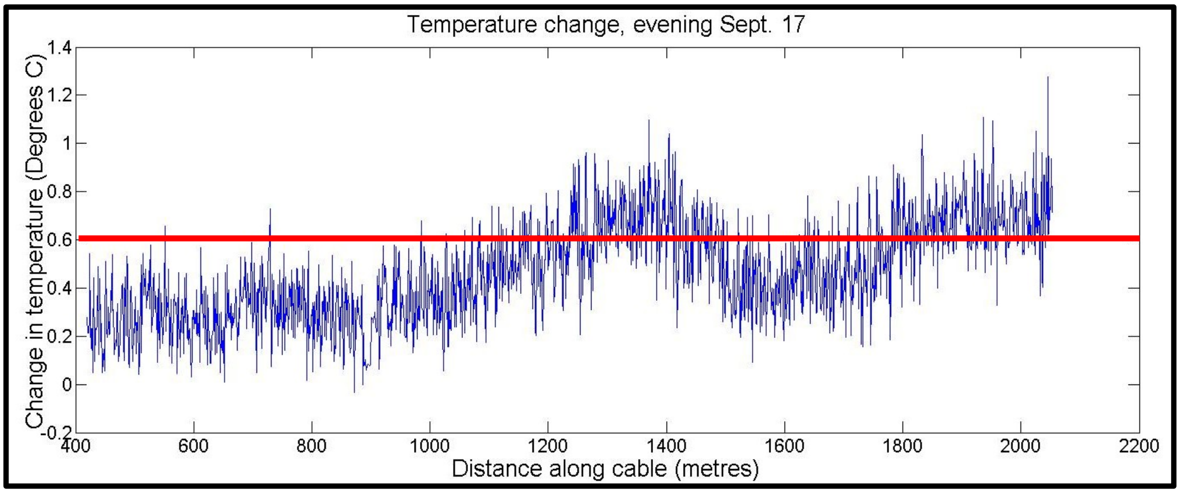

Figure 22 Change in temperature at each metre during the sudden warming on the evening of September 17. The straight line indicates the average temperature increase.

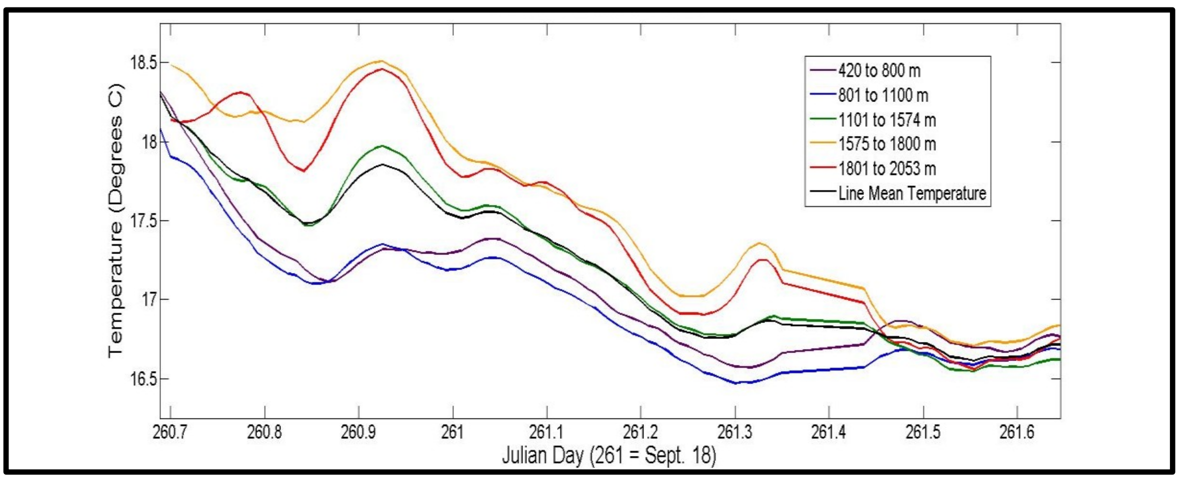

Figure 23 Temperature means for different sections of the DTS line during the standard deviation spikes on the evening of September 17 and the morning of September 18 (the 260.75 and 261.3 marks). The deeper sections of line warm briefly while the shallower sections continue to cool.

Time III

Around time III on the morning of September 18 (see Figure 20), there is a sharp peak in standard deviation and a small advance in mean temperature coinciding with a sea level low. This warming pattern is similar to the one observed at time II, except that it involves a greater length of the DTS line. The flat portion of the curve between 261.35 and 261.55 reflects the pause in data collection during which the line was georeferenced.

iBUTTONS

Of the 16 iButtons installed, one (at 10 cm sediment depth in Rod C) failed due to a software error. VFlux was run using the remaining data but results were inconsistent, with positive and negative fluxes recorded simultaneously at the same point in the case of two of the rods east of the dock (Figure 24). Rods B and C recorded continual downwards fluxes. However, the VFlux results are excluded from the interpretation. The raw data collected by the iButtons is still valid though, and the temperatures recorded by in the water column and at 15 cm sediment depth are presented in Figure 25.

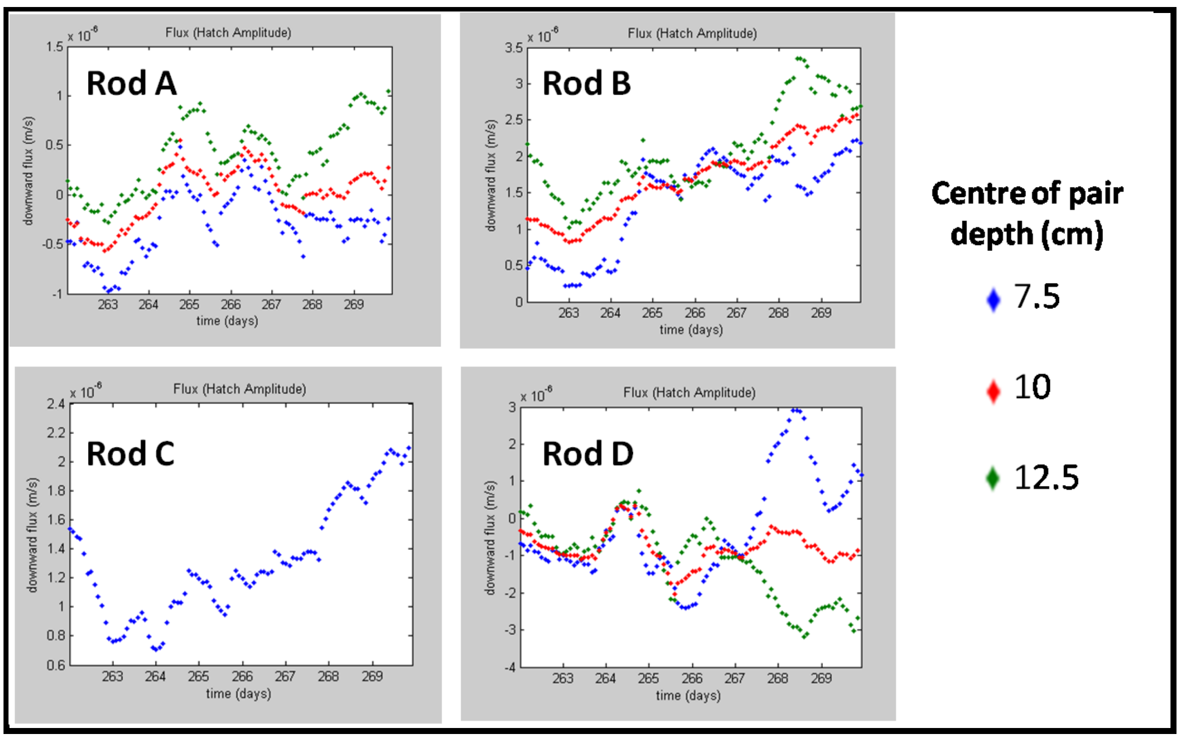

Figure 24 VFlux results for each of the iButton rods. Flux is reported at the centre of each pair of measurement points. Downward flux (10^{-6} m/s) is on the y-axis, with time in days on the x-axis.

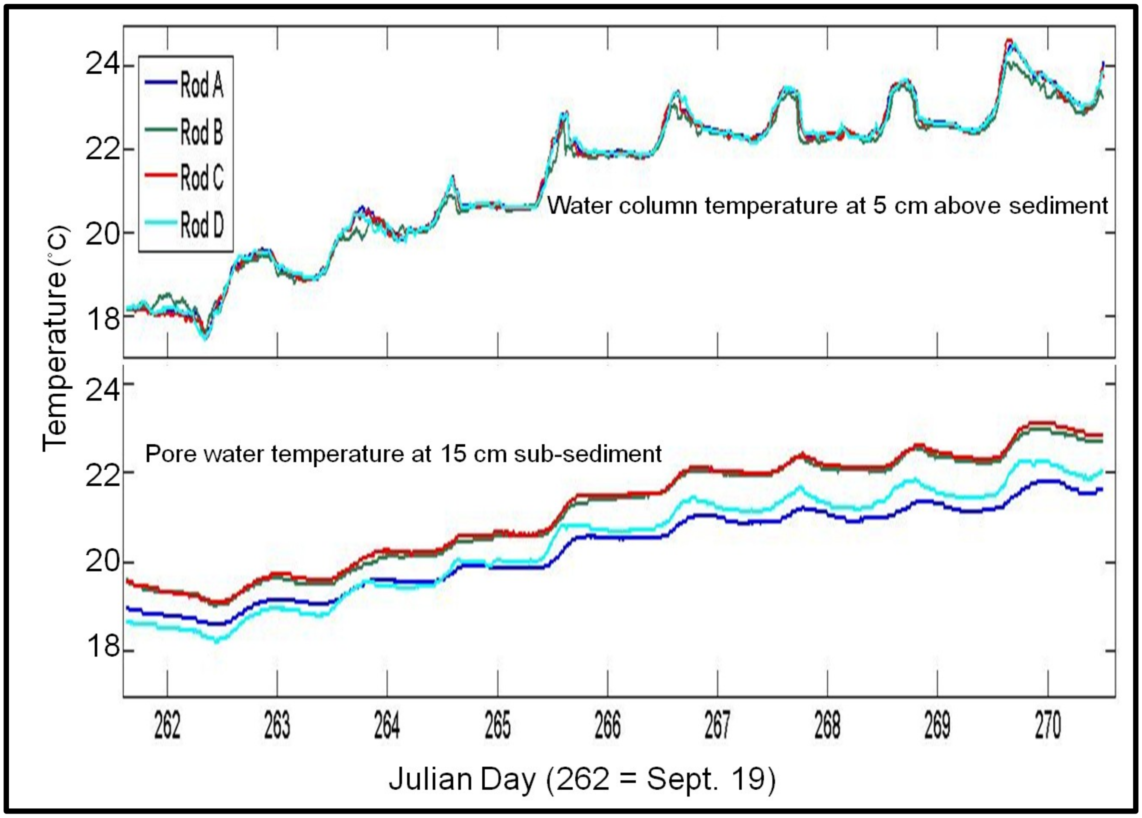

Figure 25 Temperatures measured by the top and bottom iButtons in each rod.

Discussion

From a strict mass, energy and heat capacity approach, the nearshore zone, by virtue of its shallow waters, should be more affected by diurnal warming and cooling than deeper waters. There is less water to be warmed or cooled, the sediment receives more solar radiation, and breaking waves provide relatively high interaction with the atmosphere and should allow surface waters to be readily mixed downwards. The fact that both temperature mean and variance increase with distance from shore at Holts Landing strongly suggests the influence of submarine groundwater discharge in the nearshore zone, consistent with findings in other estuary settings (eg. Michael et al. 2003). Variance increases as a power function, and begins to plateau approximately 120 m from shore. However, the DTS line only went 130 m from shore, potentially missing changes beyond that point. Low variances have previously been cited as evidence for groundwater's moderating influence in wetland streams (Lowry et al. 2007), salt marsh channels (Moffett et al. 2008) and estuaries (Henderson et al. 2009). At the beginning of the deployment, water in the nearshore zone was cooler than deeper water despite having followed at least four days of unseasonably warm weather.

East-west (i.e. shore-parallel) differences in variance were also observed. The zones between the dock and the western edge (A, B, D, H and J) all exhibited significantly lower variances than those in the extreme west (C and I) and all but one of the eastern zones. Krantz et al. (2004) suggest that the eastern and western silty zones are semi-confining and route fresh water to deeper parts of the bay. The variance findings support this, but point to another phenomenon that was not made explicit by Krantz. Namely, that the slightly overpressured margins of these buried channels can leak fresh water laterally where the silt layer is thinner, resulting in focused submarine groundwater discharge which occurs along lines which radiate from shore (Figure). This type of SGD pathway is not addressed in the most common models, which tend to orient SGD as occurring parallel to shore at various distances or at discrete points due to stratigraphy or topography (Mulligan and

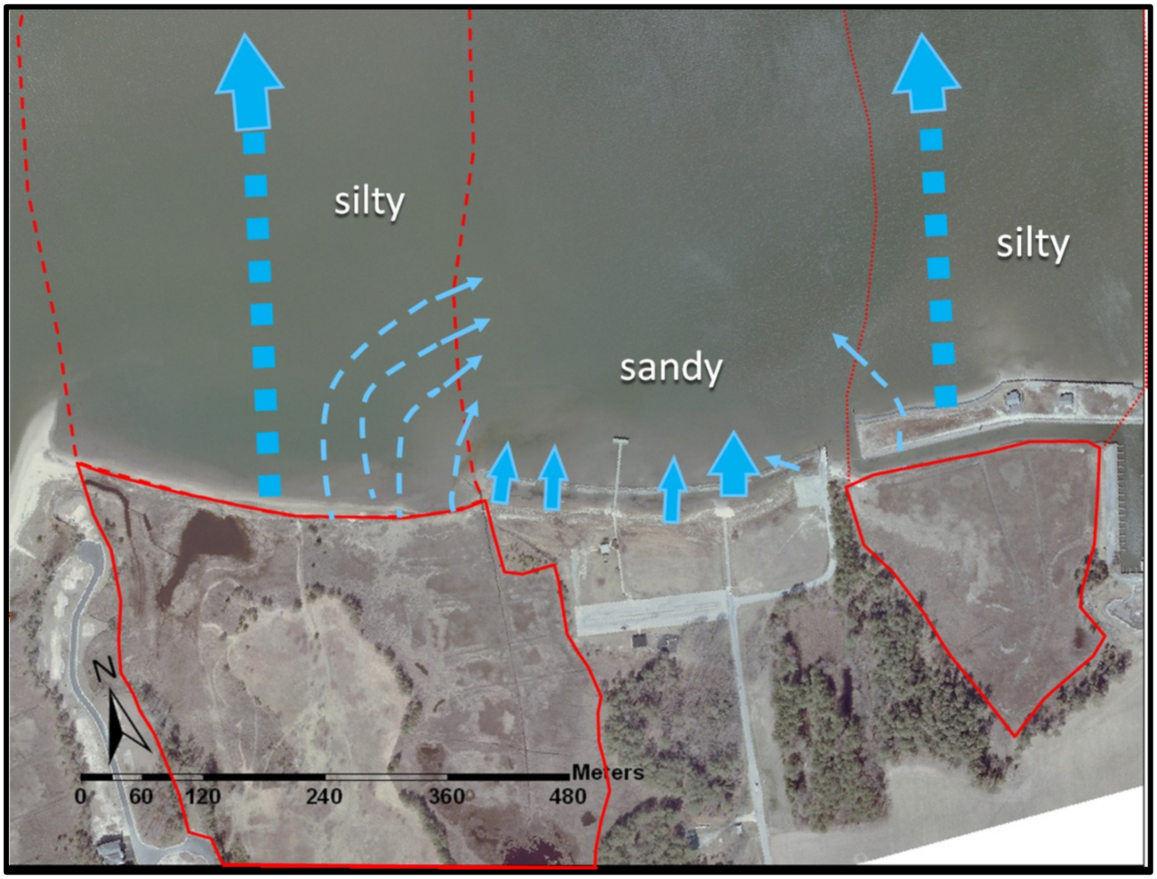

Figure 26 Conceptual model for the groundwater flow system at Holts Landing. Marshy zones on either side of the park lawn are hydraulically connected to buried submarine channels which leak water laterally into the central sandy zone. Some focused flow also occurs at the shoreline in narrow zones.

Charette, 2005), water density differences (Souza and Voss, 1987), temporal patterns or a combination of all of these (Michael et al. 2005). This likely has to do with the fact that until recently, SGD investigations relied on measurements that tended to be taken either parallel to or perpendicular to the shore. Parallel measurements provide information on the lateral location, but not the longitudinal extent, of SGD. These tend to be interpreted as springs and reported as occurring a certain distance from the coast or shoreline (eg. Taniguchi et al. 2002; Krantz et al. 2004). Measurements taken perpendicular to the shoreline where SGD is encountered tend to be interpreted as representing the situation across the breadth of the shoreline, unless there is evidence to the contrary. Experiments using a combination of point measurement configurations (lateral, longitudinal, grid or clustered) over varying extents (eg. Michael et al. 2011) attempt to overcome these limitations and address some of the scale issues raised by Bratton (2010), but still suffer from difficult implementation and sparse, discontinuous data.

DTS and other distributed measurement techniques such as infrared photography provide a means to collect high resolution, continuous temporal and spatial data and improve our understanding on the issues of scale raised by Bratton (2010). These highly organized data lend themselves to more complex computer-based analyses, and have the potential to reveal previously undetectable patterns. However, it is still important to consider how, in the case of DTS, the line is configured. The configuration here was based, in part, on the desire to compare differences along the east-west axis at Holts Landing. As such, the cable was laid out in what are essentially shore-parallel transects. While this provided tremendous information on metre-scale differences along this axis, the ability to resolve north-south differences is extremely limited. In retrospect, a gridded configuration would have been better in this setting. Not only would it provide a less skewed view of the area, it would also provide an opportunity to constrain measurement drift along the line by duplicating measurements at the points where the line crosses itself. Gridded data is also more suited to interpolation than linear data, and would be more reliable in efforts, for example, to spatially rasterize the data in order to detect or map patterns.

Previous geophysical work at Holts Landing has provided no reason to suspect that there would be differences in SGD between different parts of the central sandy zone. However, temperature at the southeast corner (zone F) was significantly more variable than in zone E only 50 m away. Mean temperatures measured by the DTS system in zones E and F are also below the cable average. The corner is close to infrastructure such as the boat ramp and breakers, which might influence groundwater flow patterns. It also potentially sits over the edge of the eastern silty zone identified during the 2004 geophysical survey. Results from the iButton rods D and A, 30 m and 150 m to the east respectively, show that while water column temperatures were tightly coupled with those at other rod locations, the pore water temperatures were cooler and recover more slowly than at rods B and C (Figure 25). Considering this, the relatively high variance at these locations (Figure 18) suggests that lower sediment permeability there is impairing tidally-driven flux into and out of the sediment, limiting heat exchange.

The narrow B and E zones demonstrate the efficacy of the DTS in locating small-scale processes in a very short time, even when conditions are less than ideal. Zone B, 8 m wide, is visible as a vertical stripe between 400 and 600 m in Figure 14. It was anomalously cold (significant, $p<0.05$) and exhibited a clear drop in standard deviation (Figure 16) although this was not statistically significant (most likely due to the small sample size). Nonetheless, something clearly changes between zones A and B, and targeted work in this area would likely reveal a source of groundwater, since the temperature cannot be explained by longshore currents, which would cool other parts of the cable. Zone E stands out from its surroundings as a clear depression on the same standard deviation plot. It is not distinguishable from the west side, where, as observed above, standard deviations are lower. It is associated with a particularly sandy zone on shore which is visible in aerial photos dating back to 1937 (Figure), and which appears to have been built up by years of sedimentation from overland flow. Such fluvial deposits from the sandy upland would have a very high hydraulic conductivity and could reasonably act as a primary route for fresh groundwater from the upgradient park to the sea. This area also borders the high-variance zone F, which is at the margin of the eastern channel detected by geophysics, but is also in the recently reworked area by the boat ramp and marina entrance. It is possible that this area behaves similarly to what has been suggested about the western flank, namely that groundwater moving through

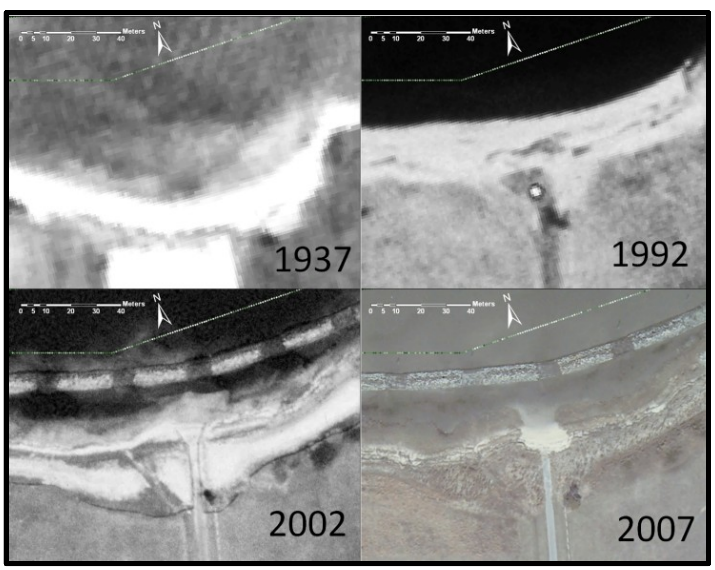

Figure 27 Orthophotos of the low-variance zone and the nearby beach area. Source: Delaware Geological Survey

a highly permeable buried channel under semi-confining sediments is squeezed out at the margins. Another possibility is that low-permeability fill used in the infrastructure projects locally inhibits horizontal groundwater movement, thereby causing surrounding areas (such as zone E) to experience greater fluxes. The lower variances observed near the dock support this infrastructure argument.

The high temperatures and low variances recorded near the end of the line might suggest that there is a highly localized phenomenon in the far northeast corner. This is unlikely, though. The signal is interpreted as interference caused either by proximity to the end splice or damage to the line (kinks) caused by handling during deployment. These few metres of line in particular were handled, pulled and turned around obstacles the most, so damage is the likely explanation.

Choosing which zones to compare was subjective. Most of the zones (with the exception of zone B) are subsets of groups that showed broad trends in either mean or variance. Because one of the goals of this project was to identify hydrologic processes, these subsets generally represent the most extreme (but spatially coherent) examples from within these groups. In other words, the intent was to divide and discover, not to discretize and organize. If the interest was to classify and group different types of zones, this approach would not be appropriate. Instead, a machine method could probably be developed to move along the string of data and detect similarities between contiguous and non-contiguous groups. However, that is beyond the scope of this project.

COMPARISON TO SEEPAGE METER RESULTS

Russoniello et al. (in preparation) used seepage meters to measure SGD and salinity in the same area covered in this study, and some of their results are summarized in Figure 28. They noted that areas with freshwater discharge had depressed levels of saline discharge, interpreted by the authors to mean that fresh SGD suppresses shallow saline water recirculation by reducing the downward hydraulic gradient into the shallow mixing zone. This finding implies that the thermal regime at the ground/water interface in SGD zones would be more representative of groundwater than SGD-free zones, supporting the validity of the assumption made earlier that SGD in tidal settings leads to lower temperature variances.

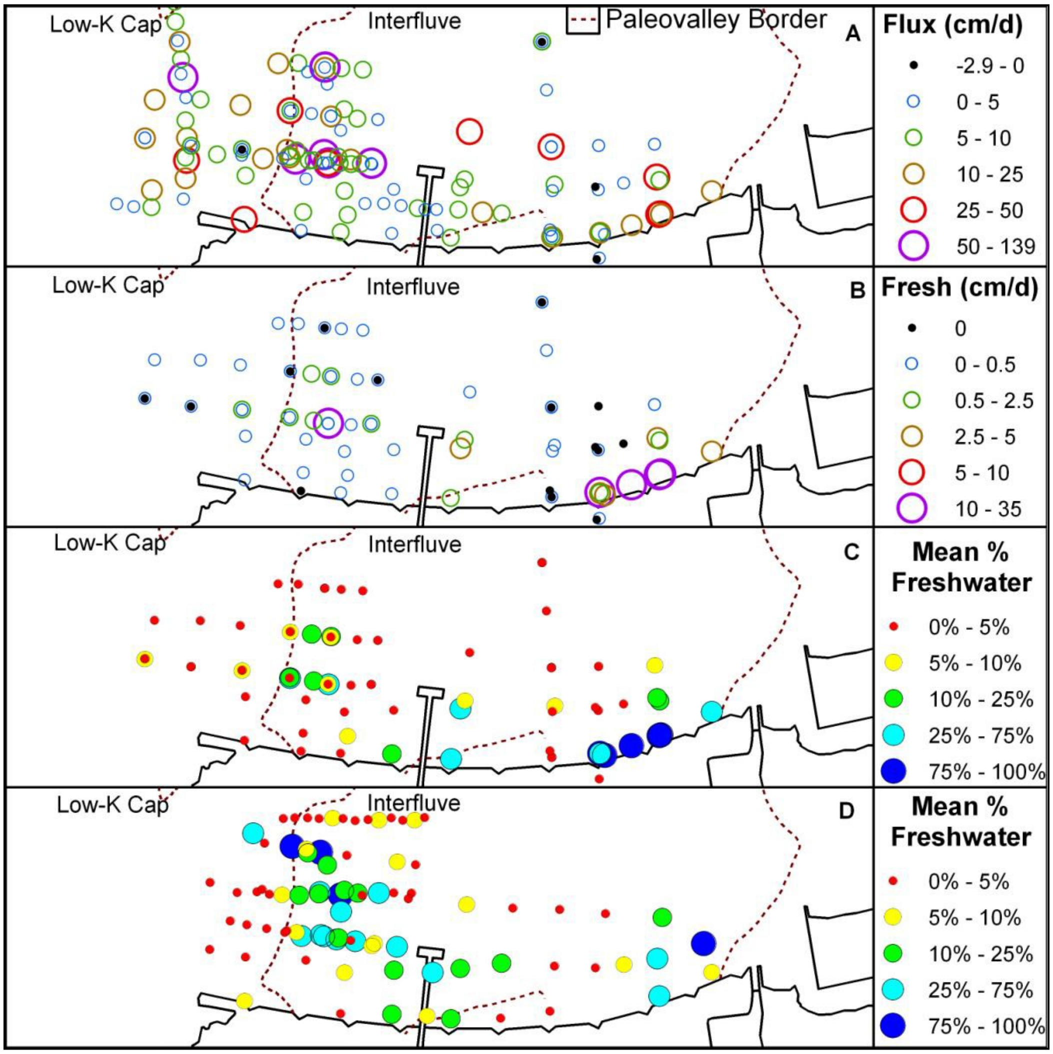

Figure 28 Seepage meter results. Panel A shows total (fresh and saline) SGD rates. B shows freshwater flux rates, C shows freshwater flux as a percentage of total SGD, and D shows percent fresh porewater as measured with a sampler. Adapted from Russoniello et al. (in preparation).

Considering that the DTS and seepage meter measurements were not taken at the same time or in the exact same locations, there is considerable agreement between the two sets of results. While there are some differences (for example freshwater discharge near deeper portions of the dock), the general pattern is clearly the same. Freshwater discharge measured by meters was generally limited to the nearshore zone of the sandy area (average 18.9% fresh), and to the area flanking the paleovalley (average 7.2% fresh). There is a distinct shift in discharge patterns between the sandy area (labelled below as the interfluve) and paleovalley to the west, reflecting the same differences observed between Zones H and I above. The cluster of high percent-fresh discharge at the eastern portion of the near-shore zone in Figure 28 corresponds to Zone E. Taken together, the two sets of results support the hypothesis that SGD patterns are controlled to some extent by the distribution of sediment on the bay floor, and can therefore tell us something about the hydrogeology of the site. They also demonstrate the efficacy of gathering data with DTS, which, in a three-day deployment, provided the same overall qualitative picture as two years of seepage meter data.

WATER LEVELS AND TEMPERATURE

Although changing water levels contribute to temperature changes, they are secondary to diurnal forcing (see Figure 31) and it is difficult to attribute specific phenomena to them, especially when the system changes as rapidly as it did here. However, some observations can be made. Immediately after each low water stand during the DTS deployment, the slope of the temperature graph became more positive, if only briefly and slightly, across the entire line (Figure 23). In other words, it appears that the majority of the cooling occurred as pore pressures at the sediment/water interface decreased, and that cooling was suppressed as water column pressures increased. It also appears that the areas that responded most strongly to this were the deeper ones. This can be seen as evidence that as temperatures fell across the system the warmer water was being pushed out from shore gradually by cold water in tidal pulses, as opposed to having colder water pushed in from the open bay. The patterns at times II and III described in the results section above can be attributed directly to this. It is not clear whether the cold water here is groundwater, direct runoff from the storm system, indirect surface runoff brought in via littoral processes or shallower bay water cooled by interaction with the atmosphere.

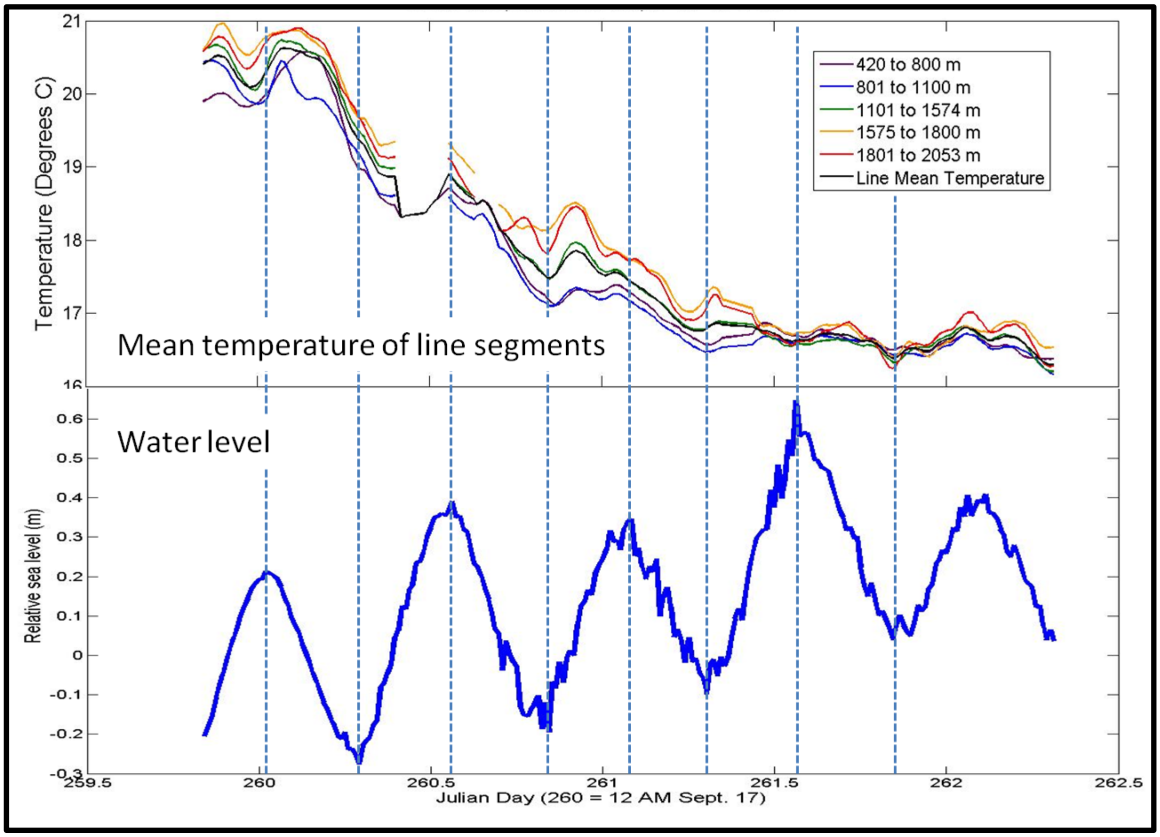

Figure 29 Estuary water levels and their relationship to temperature changes.

The sudden 0.7°C rise in temperature across the line accompanied by a drop in standard deviation at around midnight on September 17 (mark 260, Figure 20) appears to have been caused by tidal-related warming in areas that coincide with higher-variance zones. A possible explanation is that the very warm tide coinciding with the DTS deployment ran up and, due to head differences, inhibited the SGD from its source in the low-variance zones. As the tide retreated, the entire area continued to draw heat from the warm overlying water. However, the dropping pressures would have once again permitted SGD to occur, moderating the temperature increase in low-variance zones. The most distal zone (after 1600 m) experienced less heating because it was already very warm (Figure 30). Burnett et. al (2006) observed similar patterns, with maximum SGD occurring at low tides.

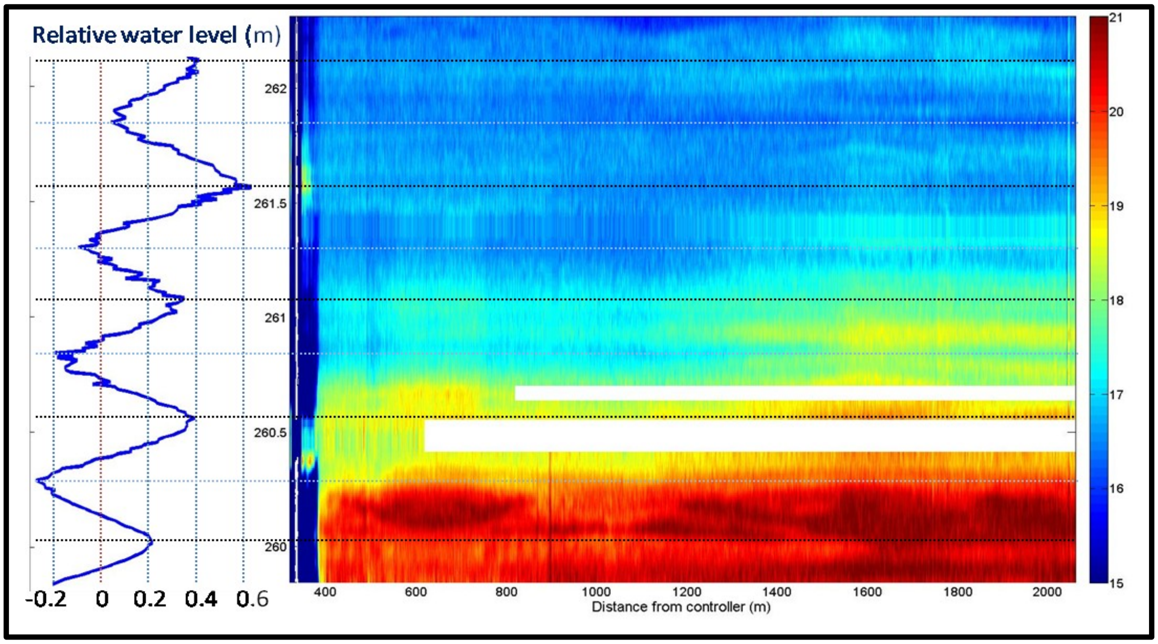

Figure 30 Water level shown in relation to the DTS dataset. Dark lines are high tides, light are low.

VERTICAL POREWATER FLUX

VFlux was ineffective in this particular set of circumstances. The consistent downwards flux calculated for rods B and C is highly unlikely given the decreasing water levels during the iButton deployment which, if anything, should have resulted in a flushing of porewater in response to lower hydrostatic pressures. As mentioned in the results section, the flux calculations from Rods A and D are equally suspect. The Hatch method relies on a clean sinusoidal temperature signal, which VFlux generates from the raw data using dynamic harmonic regression, regardless of the quality of that raw data. In other words, usable sinusoidal temperature signals can be generated from extremely poor non-sinusoidal raw data.

A quick test shows that this is not the fault of the authors of VFlux. For example, the water column temperature record from rod D was detrended and then analyzed using the Discrete Fourier Transform (fft) function in MATLAB. The top 10 component frequencies were identified, the top two of which were the 24-hour diurnal signal and the 12.63-hour tidal signals, calculated respectively as 23.24 and 12.78 hours. The frequencies were then reassembled into a synthetic dataset. The results, shown in Figure 31 are compared to the original data, with very poor overlap. Amplitudes are underestimated and many of the peaks are split in two. This is likely due to a combination of factors, including a short sampling period, a (curved) positive temperature trend, inconsistent, strangely shaped temperature peaks, and the coincidence of the tidal and diurnal signals, which are nearly multiples of each other. Hatch et al. (2006) also warn that the method is extremely sensitive to rapid changes in the magnitude and direction of flux. It is therefore possible that the tide's sub-daily influence on SGD is, by itself, enough to disrupt the calculation. It may be that the method is not well-suited to those tidal areas where the hydrostatic pressure changes are sufficient to interrupt SGD.

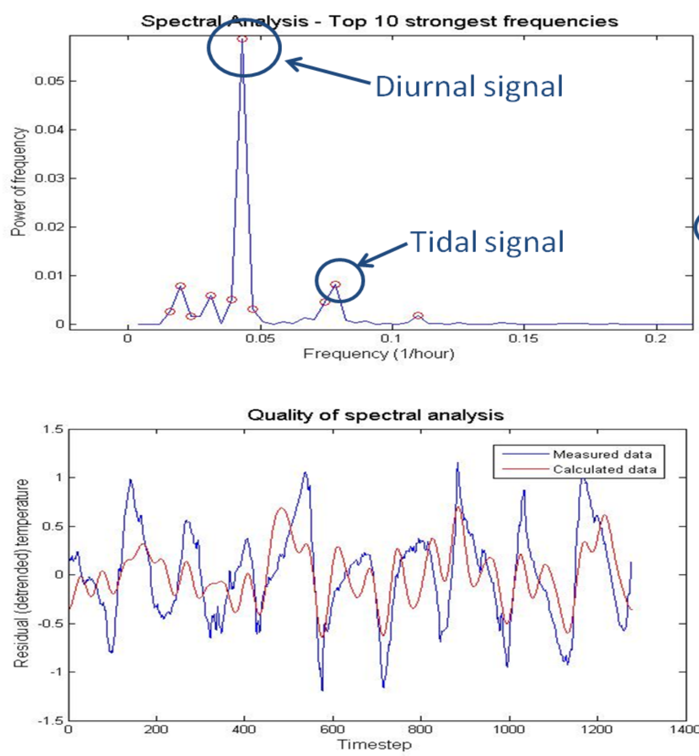

Period (Hours)	n
23.24	10
12.78	19
51.12	4
31.95	7
25.56	9
13.45	18
21.30	11
63.90	3
9.13	27
42.60	5

Figure 31 Top ten component frequencies identified in the water temperature at rod D. The red line in the bottom graph is the composite of the extracted frequencies, while the blue line is the original data.

While negative results are not typically reported in the literature, the practice is growing out of an interest to publish failed attempts at results replication and prevent replication of mistakes or dead ends in research (Dirnagl, 2010; Giraud-Carrier, 2010). It is useful in this case to point out that there are limitations to the Hatch method as implemented in VFlux. In particular, because the software is so straightforward to use, cleans up the signal and always provides a result, it is easy to accept the output it provides as valid. Caution should be exercised, though, when interpreting the results.

The iButton data do suggest that water temperatures just a few centimetres above the bay floor change uniformly, regardless of location. The only obvious difference in the top section of Figure 25 is that the water temperature at rod B, which is further from shore than the other three rods, does not reach the same daily peaks as the others while the system warms up. This is puzzling, given the inversion of the relationship between temperature and distance from shore seen in the DTS data. In addition, pore water temperature at B is the same as at rod C, eliminating the possibility that this is due to different groundwater temperatures. On day 262, when pore water was warmer than the surface water, rod B's surface water temperature was higher than all of the other rods. This indicates two possibilities. The first is that the rod was placed in more permeable sediments than the others, resulting in higher SGD throughout the deployment. The other possibility is that when the rod was installed, the sediment was disturbed to the point that groundwater could easily flow out around the rod, cooling or warming the iButton. Rod B was installed on the boundary between the low-variance zone west of the mid-dock and the high variance zone near the dock. Without more information it is impossible to determine which of the above scenarios is more likely. In either case, though, it appears that groundwater plays a role.

The breaks in the DTS line resulted in the complete loss of some data and sufficient doubt in other data (for example, in the areas immediately after metres 890 and 1742, for the duration of the experiment) so as to render it unusable. The cable used in this deployment is military-grade, with the glass fibres protected in gel inside a small extruded steel capillary which is then wrapped in braided steel and protective plastic sheathing. It has high tensile strength and is very resistant to being knocked, even with rocks. However, when the cable is bent too sharply it kinks. When this happens the capillary tube can snap, creating sharp edges which easily sever the glass fibres, even when the outside of the cable is undamaged. It is worth considering whether or not such a robust but expensive and inflexible cable is the best choice in low kinetic energy settings such as the estuary at Holts Landing. There are options available for waterproof fibre-optic lines that use semi-rigid materials which would be less prone to breaks during handling (paying out or retracting line), which is when most of the damage occurs. Another consideration is how frequently the line is expected to be used. Longer, less frequent deployments may benefit from heavy duty cable but frequent, brief studies in calm environments such as this one may do better with lighter, more flexible line.

In the context of Indian River Bay, the conceptual model proposed above raises some interesting questions. When viewed as a part of the larger shoreline, the marsh and the sandy lawn at Holts Landing fit into a larger pattern of what appear to be marshes (Figure 32, outlined in red) alternating with slightly elevated, developed or managed land. The implication here is that bands of three different types of water radiate from shore. Immediately offshore from the marsh areas we could expect well-mixed, average bay water largely unaffected by SGD. Near the developed zones we could expect a mix of bay water and SGD deriving from the developed areas. Between these zones we would expect to see both of these types, mixed with very fresh upland water which moves via the buried channels and subsequently discharges to the estuary near shore. Since our data was limited to within 130 m of shore, it is difficult to say what happens beyond that. However, Krantz et al. (2004) suggest that the buried channels carry fresh water out as far as 1 km. This means that managers concerned with nutrient or contaminant transport in the region must consider a system that spans at least two of the scales that Bratton (2010) describes.

Another implication is that, because the semi-confining sediments offshore of the marsh areas appear to be very thin, any disturbance to these areas (for example, by infrastructure projects), could cause sudden major changes to groundwater flowpaths into and under the bay. In the longer-term, land use changes such as on-shore development projects, by virtue of stabilizing soil and channeling runoff, could significantly alter erosional/depositional regimes in the bay. This could have the effect of making the buried channels more or less leaky, and result in a complete shift in how, where, and how quickly groundwater moves into the estuary. Such potential changes have important ecological, social, economic and policy implications.

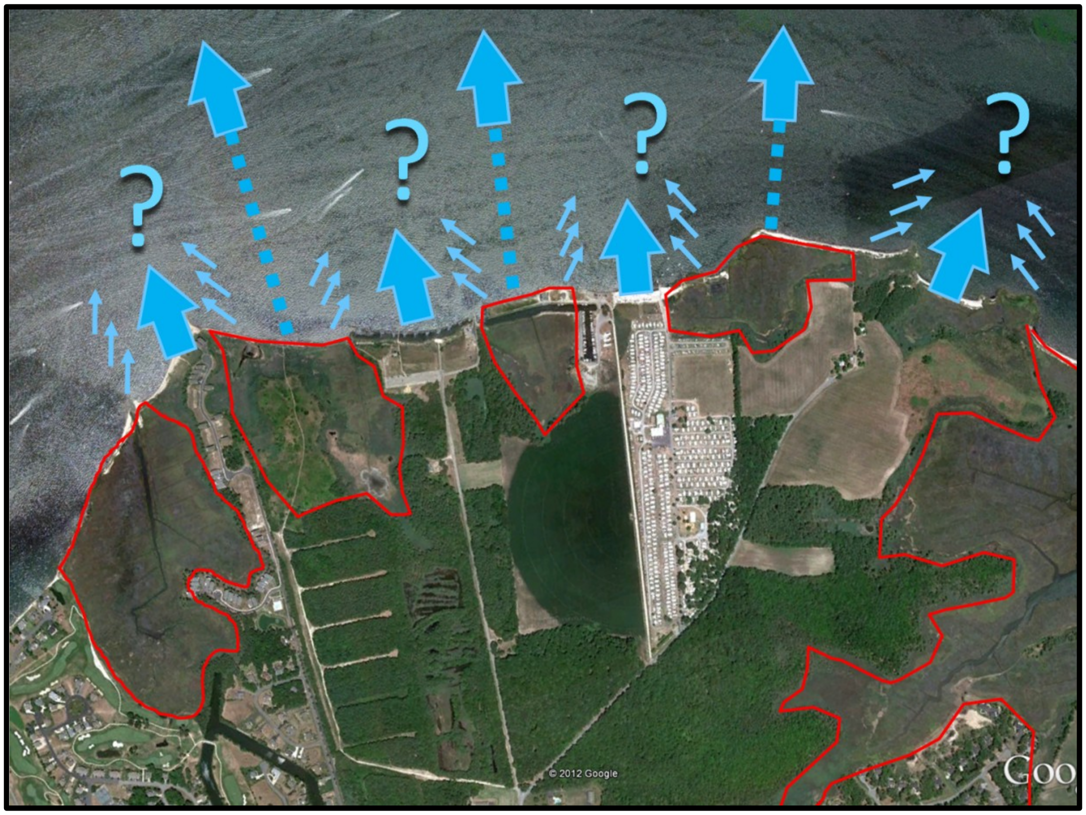

Figure 32 The conceptual model presented in Figure , expanded to a larger section of the Indian River Bay shoreline. Source: Google Maps

Conclusion

Distributed temperature data show that the waterfront at Holts Landing State Park is a hydrogeologically heterogeneous system. Temperature variance decreases with distance from shore, suggesting that the influence of SGD plateaus approximately 120 m from shore. However, this was near the limits of the deployment zone and it is possible that processes further out were missed. Spatially grouped low variances are interpreted as being the result of temperature moderation by groundwater.

In this study, the failure to estimate flux based on vertical temperature profiles is a serious limitation and it is therefore difficult to make definitive statements about groundwater entering the local estuary system. However, the spatial and temporal temperature patterns observed here suggest that groundwater is entering the estuary in different ways. Variance and mean temperature imply zones of focused flow near the shore, reduced flow along the eastern and western flanks, and spatially organized diffuse flow at the periphery of the silty western flank, extending bayward. This last type of flow organization has not been described to my knowledge in the literature, and would not be readily detectable using non-distributed measurement approaches.

Tidal forcing was responsible for some of the observed patterns. There is strong evidence that the second largest spike in standard deviation calculated across the whole line is the direct result of the turning of a tide.

VFlux, the automated script for calculating groundwater flux between vertically-aligned temperature loggers, did not produce reasonable results in this setting. This is likely caused by non-sinusoidal temperature signal, a warming trend which lasted the duration of the experiment, and tidal and diurnal frequencies which happened to be tightly coupled. It is also possible that tidal forcing on its own is enough to disrupt flux calculations, and that this method is not well-suited for some tidal environments.

Poor weather and equipment failures interfered with data collection, but this could have been at least partially avoided had the DTS line been handled with more caution. It is recommended that researchers interested in using fibre-optic DTS consider cable options that may not be as robust but are best suited to the job at hand. In low-energy settings, a more flexible cable may be better than a more rigid, protective one.

Distributed temperature sensing was also effective in the sense that in three days over a million data points were collected over 55,000m^2. This data is highly organized, and is conducive to machine analysis, which could easily be used to optimize the detection of similarities and differences between groups of points.

Based on this and other studies, it seems apparent that SGD paths at Holts Landing are controlled by small yet important differences in the bay floor sediment. Any changes to the sedimentary system by direct or indirect action could have important implications for the location, amount and quality of submarine groundwater discharge into the Indian River Bay estuary.

REFERENCES

Alexander, C., Smith, R., Loganathan, B., Ertel, J., Windom, H.L., Lee, R.F. 1999. Pollution history of the Savannah River estuary and comparisons with Baltic Sea pollution history. Limnologica - *Ecology and Management of Inland Waters* 29, 267–273.

Andres, A.S. 1991. Results of the coastal Sussex County, Delaware ground-water quality survey. Newark, DE: Delaware Geological Survey, University of Delaware.

Andres, A.S. 1992. Estimate of nitrate flux to Rehoboth and Indian River bays, Delaware, through direct discharge of ground water. Newark, DE: Delaware Geological Survey, University of Delaware.

Bear JA, Cheng HD, Sorek S, Ouuzar D, Herrera I, editors. 1999. Seawater intrusion in coastal aquifers — concepts, methods and practices. Dordrecht, the Netherlands: Kluwer Academic Publishers; 625 pp.

Bratton, J.F., Bohlke, J.K., Manheim, F.T., Krantz, D.E. 2004. Ground Water Beneath Coastal Bays of the Delmarva Peninsula: Ages and Nutrients. *Ground Water* 42, 1021–1034.

Burnett, W.C., Aggarwal, P.K., Aureli, A., Bokuniewicz, H., Cable, J.E., Charette, M.A., Kontar, E., Krupa, S., Kulkarni, K.M., Loveless, A., Moore, W.S., Oberdorfer, J.A., Oliveira, J., Ozyurt, N., Povinec, P., Privitera, A.M.G., Rajar, R., Ramessur, R.T., Scholten, J., Stieglitz, T., Taniguchi, M., Turner, J.V. 2006. Quantifying submarine groundwater discharge in the coastal zone via multiple methods. *Science of The Total Environment* 367, 498–543.

Cable, J.E., Martin, J.B. 2008. In situ evaluation of nearshore marine and fresh pore water transport into Flamengo Bay, Brazil. *Estuarine, Coastal and Shelf Science* 76, 473–483.

Cerco, C.F., Bunch, B., Cialone, M.A., Wang, H. 1994. Hydrodynamics and eutrophication model study of Indian River and Rehoboth Bay, Delaware. Technical Report EL-94-5, United States Army Engineer Waterways Experiment Station, Vicksburg, Mississippi.

Cerco, C.F., Seitzinger, S.P. 1997. Measured and Modeled Effects of Benthic Algae on Eutrophication in Indian River-Rehoboth Bay, Delaware. Estuaries 20, 231.

Dakin, J.P., Pratt, D.J., Bibby, G.W., Ross, J.N. 1985. Distributed optical fibre Raman temperature sensor using a semiconductor light source and detector. *Electronics Letters* 21, 569–570.

Delaware Geological Survey. 2012. Orthophotos of the Holts Landing State Park area. http://datamil.delaware.gov/tiles/. Tile 1698. Accessed Mar. 6, 2012.

Denver, J.M., Ator, S.W., Debrewer, L.M., Ferrari, M.J., Barbaro, J.R., Hancock, T.C., Brayton, M.J., Nardi, M.R. 2004. Water quality in the Delmarva Peninsula. U.S. Geological Survey Circular No. 1228. Reston, VA.

Dillow, J.J.A., Greene, E.A. 1999. Groundwater Discharge and Nitrate Loadings to the Coastal Bays of Maryland. USGS Water-Resources Investigations Report No. WRIR-99-4167. U.S. Geological Survey, Baltimore, MD.

Dimova, N.T., Swarzenski, P.W., Dulaiova, H., Glenn, C.R. 2012. Utilizing multichannel electrical resistivity methods to examine the dynamics of the fresh water–seawater interface in two Hawaiian groundwater systems. *Journal of Geophysical Research* 117.

Dirnagl, U., Lauritzen, M. 2010. Fighting publication bias: introducing the Negative Results section. Journal of Cerebral Blood Flow and Metabolism 30, 1263–1264.

Duarte, T.K., Pongkijvorasin, S., Roumasset, J., Amato, D., Burnett, K. 2010. Optimal management of a Hawaiian coastal aquifer with nearshore marine ecological interactions. *Water Resources Research* 46.

Feced, R., Farhadiroushan, M., Handerek, V.A., Rogers, A.J. 1997. Advances in high resolution distributed temperature sensing using the time-correlated single photon counting technique. *Optoelectronics, IEE Proceedings* 144, 183–188.

Fleury, P., Bakalowicz, M., de Marsily, G. 2007. Submarine springs and coastal karst aquifers: A review. *Journal of Hydrology* 339, 79–92.

Giraud-Carrier, C., Dunham, M.H., Atreya, A., Elkan, C., Perlich, C., Swirszcz, G., Shi, X., Philip, S.Y., Fürnkranz, J., Sima, J.F., others, 2010. On the importance of sharing negative results. *SIGKDD explorations* 12, 3–4.

Gordon, R.P., Lautz, L.K., Briggs, M.A., McKenzie, J.M. 2012. Automated calculation of vertical pore-water flux from field temperature time series using the VFLUX method and computer program. *Journal of Hydrology* 420-421, 142–158.

Groot, J.J., Ramsey, K.W., Wehmiller, J.F. 1990. Ages of the Bethany, Beaverdam, and Omar formations of southern Delaware (Report of Investigations No. 47). Delaware Geological Society, University of Delaware, Newark, DE.

Hartog, A.H., Leach, A.P., Gold, M.P. 1985. Distributed temperature sensing in solid-core fibres. *Electronics Letters* 21, 1061–1062.

Hatch, C.E., Fisher, A.T., Revenaugh, J.S., Constantz, J., Ruehl, C. 2006. Quantifying surface water–groundwater interactions using time series analysis of streambed thermal records: Method development. *Water Resources Research* 42, W10410.

Henderson, R.D., Day-Lewis, F.D., Harvey, C.F. 2009. Investigation of aquifer-estuary interaction using wavelet analysis of fiber-optic temperature data. Geophysical Research Letters 36, L06403.

Hubbert, M.K. 1940. The theory of ground-water motion. The Journal of Geology 785–944.

Johannes, R.E. 1980. Ecological significance of the submarine discharge of groundwater. *Marine Ecology-Progress Series* 3, 365–373.

Kennish, M.J. 2000. Estuary Restoration and Maintenance: The National Estuary Program. Boca Raton, FL: CRC Press; 359 pp

Kim, G., Lee, K.K., Park, K.S., Hwang, D.W., Yang, H.S. 2003. Large submarine groundwater discharge (SGD) from a volcanic island. *Geophysical Research Letters* 30, 2098.

Kohout, F.A. 1966. Submarine springs: a neglected phenomenon of coastal hydrology. *Hydrology* 26: 391–413

Krantz, D.E., Manheim, F.T., Bratton, J.F., Phelan, D.J. 2004. Hydrogeologic Setting and Ground Water Flow Beneath a Section of Indian River Bay, Delaware. *Ground Water* 42, 1035–1051.

Lapham, W.W. 1989. Use of temperature profiles beneath streams to determine rates of vertical ground-water flow and vertical hydraulic conductivity. US Geological Survey Water Supply Paper 2337; 35 pp.
Lautz, L.K. 2010. Impacts of nonideal field conditions on vertical water velocity estimates from streambed temperature time series. *Water Resources Research* 46, W01509.
Lee, D.R. 1977. A Device for Measuring Seepage Flux in Lakes and Estuaries. *Limnology and Oceanography* 22, 140–147.
Lee, D.R., Cherry, J.A. 1978. A field exercise on groundwater flow using seepage meters and mini piezometers. *Journal of Geological Education* 27, 6–10.
Lowry, C.S., Walker, J.F., Hunt, R.J., Anderson, M.P. 2007. Identifying spatial variability of groundwater discharge in a wetland stream using a distributed temperature sensor. *Water Resources Research* 43, W10408.
Manheim, F.T., Krantz, D.E., Bratton, J.F. 2004. Studying ground water under Delmarva coastal bays using electrical resistivity. *Ground Water* 42, 1052–1068.
McCoy, C.A., Corbett, D.R., McKee, B.A., Top, Z. 2007. An evaluation of submarine groundwater discharge along the continental shelf of Louisiana using a multiple tracer approach. *Journal of Geophysical Research* 112, C03013.
Michael, H.A., Charette, M.A., Harvey, C.F. 2011. Patterns and variability of groundwater flow and radium activity at the coast: A case study from Waquoit Bay, Massachusetts. *Marine Chemistry* 127, 100–114.
Michael, H.A., Lubetsky, J.S., Harvey, C.F. 2003. Characterizing submarine groundwater discharge: A seepage meter study in Waquoit Bay, Massachusetts. *Geophysical Research Letters* 30, 1297.
Michael, H.A., Mulligan, A.E., Harvey, C.F. 2005. Seasonal oscillations in water exchange between aquifers and the coastal ocean. *Nature* 436, 1145–1148.
Moffett, K.B., Tyler, S.W., Torgersen, T., Menon, M., Selker, J.S., Gorelick, S.M. 2008. Processes controlling the thermal regime of saltmarsh channel beds. *Environmental Science & Technology* 42, 671–676.
Mondal, N.C., Singh, V.P., Singh, V.S., Saxena, V.K. 2010. Determining the interaction between groundwater and saline water through groundwater major ions chemistry. *Journal of Hydrology* 388, 100–111.
Mulligan, A.E., Charette, M.A. 2006. Intercomparison of submarine groundwater discharge estimates from a sandy unconfined aquifer. *Journal of Hydrology* 327, 411–425.
NCDC (National Climatic Data Center). Website. 1981-2010 US normals data. Accessed Feb. 4, 2012. http://gis.ncdc.noaa.gov/map/cdo/?thm=themeNormals
Oertel, G.F. 1985. The barrier island system. Marine Geology 63, 1–18.
Peterson, B., Stubler, A., Wall, C., Gobler, C. 2012. Nitrogen-rich groundwater intrusion affects productivity, but not herbivory, of the tropical seagrass Thalassia testudinum. *Aquatic Biology* 15, 1–9.
Rao, A.M.F., Charette, M.A. 2012. Benthic Nitrogen Fixation in an Eutrophic Estuary Affected by Groundwater Discharge. *Journal of Coastal Research* 280, 477–485.
Rapaglia, J., Koukoulas, S., Zaggia, L., Lichter, M., Manfé, G., Vafeidis, A.T. 2012. Quantification of submarine groundwater discharge and optimal radium sampling distribution in the Lesina Lagoon, Italy. *Journal of Marine Systems* 91, 11–19.

Russoniello, C.J., Fernandez, C., Bratton, J.F., Banaszak, J., Krantz, D., Andres, A.S., Konikow, L.F., Michael, H.A. In Preparation. Geologic controls on groundwater salinity and discharge into Indian River Bay, Delaware.

Selker, J.S., Thévenaz, L., Huwald, H., Mallet, A., Luxemburg, W., van de Giesen, N., Stejskal, M., Zeman, J., Westhoff, M., Parlange, M.B. 2006. Distributed fiber-optic temperature sensing for hydrologic systems. *Water Resources Research* 42, W12202.

Simmons Jr, G.M. 1992. Importance of submarine groundwater discharge(sgwd) and seawater cycling to material flux across sediment/water interfaces in marine environments. *Marine Ecology Progress Series* 84, 173–184.

Slater, L.D., Ntarlagiannis, D., Day-Lewis, F.D., Mwakanyamale, K., Versteeg, R.J., Ward, A., Strickland, C., Johnson, C.D., Lane, J.W. 2010. Use of electrical imaging and distributed temperature sensing methods to characterize surface water–groundwater exchange regulating uranium transport at the Hanford 300 Area, Washington. *Water Resources Research* 46, W10533.

Souza, W.R., Voss, C.I. 1987. Analysis of an anisotropic coastal aquifer system using variable-density flow and solute transport simulation. *Journal of Hydrology* 92, 17–41.

Stallman, R.W. 1965. Steady one-dimensional fluid flow in a semi-infinite porous medium with sinusoidal surface temperature. *Journal of Geophysical Research* 70, 2821–2827.

Stonestrom, D.A., Constantz, J.E. 2003. Heat as a tool for studying the movement of ground water near streams (USGS Circular No. 1260). US Dept. of the Interior, US Geological Survey, Reston, Va.

Striegl, A.M., Loheide, S.P. 2012. Heated Distributed Temperature Sensing for Field Scale Soil Moisture Monitoring. *Ground Water* 50, 340-347.

Taniguchi, M., Burnett, W.C., Cable, J.E., Turner, J.V. 2002. Investigation of submarine groundwater discharge. *Hydrological Processes* 16, 2115–2129.

Taniguchi, M., Sharma, M.L. 1993. Determination of groundwater recharge using the change in soil temperature. *Journal of Hydrology* 148, 219–229.

Tyler, S.W., Selker, J.S., Hausner, M.B., Hatch, C.E., Torgersen, T., Thodal, C.E., Schladow, S.G. 2009. Environmental temperature sensing using Raman spectra DTS fiber-optic methods. Water Resources Research 45, W00D23.

APPENDIX A – CORRECTING DRIFT

```
%This code corrects DTS data for instrument drift using temperature from iButtons taped
%to the DTS loop submerged %in an ice bath.

%Data used
IceBathMean %Mean of two submerged iButtons
DelDTS.tempdata %Raw DTS temperature measurements
DelDTS.juliandate %DTS sampling dates and time

%Extract all DTS measurements from icebath loop
temp=DelDTS.tempdata(:,334:339)

%Calculate mean temperature for every measurement, across entire submerged loop
DTSIceMean=mean(temp')

%Interpolate iButton samples to fit the DTS sampling interval and timespan
ibuttonMatched=interp1(IceBathMean(:,1),IceBathMean(:,2),DelDTS.juliandate,'linear');

%Calculate correction factor
CorrectionFactor=DTSIceMean-ibuttonMatched

%Calculate correction factor
CorrectionFactor=DTSIceMean(:,2)-new_ibutton;

%Loop through each row and subtract the correction factor from each value
for i=1:278
corr_tempdata(i,:)=DelDTS.tempdata(i,:)-CorrectionFactor(i);
end
```

APPENDIX B – SMOOTHING SCRIPT

```
%This code runs a one or two-pass smoothing filter (user-defined) using a
%sliding window of 5 rows, one column at a time.It treats values within 2
%rows of an NaN as end or near-end values.

source=DelDTS.tempdata;         %User: set source equal to the table requiring
                                 %smoothing.
pass=source;                    %Creates a template matrix from the one you're
                                 %smoothing
[rows,cols]=size(source);       %Read the size of the matrix and create variables 'rows'
and 'cols'

for passnum=1:2                 %Iterate through passes.

    source=pass;

    for column=1:cols           %Begin current pass. Iterate until each column is done.

        i=1;                    %Initial value, so it's averaged only with following
values
        pass(i,column)=(source(i,column)*2 + source(i+1,column) + source(i+2,column) )/4;

        i=2;                    %Near-initial value, so its averaged is weighted towards
following values
        pass(i,column)=(source(i-1,column)* 1.5 + source(i,column) *1.5 +
source(i+1,column)+ source(i+2,column))/5;

        i=rows-1;               %Near-terminal value, with average is weighted towards
preceding values
        pass(i,column)=(source(i+1,column)* 1.5 + source(i,column) *1.5 + source(i-
1,column)+ source(i-2,column))/5;

        i=rows;                 %Terminal value, so it's averaged only with preceding
values
        pass(i,column)=(source(i,column)*2 + source(i-1,column) + source(i-2,column) )/4;

        %The following for loop handles the remaining non-end rows
        for i=3:(rows-2)
            if isnan(source(i,column))continue                              %Leave NaNs
as is.
            elseif isnan(source(i+2,column))                                %Process
numbers that precede an NaN by two or fewer rows
               if isnan(source(i+1,column))                                 %Screen for
numbers adjacent to the NaN
                    pass(i,column)=(source(i,column)*2 + source(i-1,column) + source(i-
2,column) )/4;   %Treat as a terminal value
               else pass(i,column)=(source(i+1,column)* 1.5 + source(i,column) *1.5 +
source(i-1,column)+ source(i-2,column))/5; %Treat as a near-terminal value
               end
            elseif isnan(source(i-2,column))                                %Process
numbers that follow an NaN by two or fewer rows
                if isnan(source(i-1,column))                                %Screen for
numbers adjacent to the NaN
                     pass(i,column)=(source(i,column)*2 + source(i+1,column) +
source(i+2,column) )/4;  %Treat as a beginning value
                else pass(i,column)=(source(i-1,column)* 1.5 + source(i,column) *1.5 +
source(i+1,column)+ source(i+2,column))/5;    %Treat as a near-beginning value
                end
            else pass(i,column)=(source(i-2,column)+ source(i-1,column)+
source(i,column)+ source(i+1,column)+ source(i+2,column))/5; %Run traditional five-row
window
            end
        end
    end

end
pass1=source;                 %output results of first smoothing
pass2=pass;                   %output results of second smoothing
```